BULGARIAN ACADEMY OF SCIENCES

INSTITUTE OF POLYMERS

Erik Vasilev Dimitrov

Macromolecular Design and Synthetic Strategies for the Preparation of Polymers for Delivery of Biologically Active Substances and Oligonucleotides

DISERTATION ABSTRACT

presented for acquisition of the Educational and scientific degree "**DOCTOR**"

Professional field: 4.2. Chemical Sciences

Specialty: Polymers and Polymer materials

Scientific supervisors: Prof. Stanislav Rangelov

Assos. Prof. Natalia Toncheva-Moncheva

Sofia, 2026

The dissertation was discussed and admitted for defense at a meeting of the Colloquium of the Institute of Polymers – BAS. The dissertation is presented on 181 pages and includes 137 figures, 61 schemes and 14 tables. 154 references are used. Part of the results are reported in 2 publications and 15 science forums.

The defense of the dissertation will take place on ..…….. 2026 at …….. h in the meeting room of the Institute of Polymers – BAS at a meeting of the scientific jury.

The defense materials are available to the interested ones in the office of the Institute of Polymers – BAS; Sofia, Akad. G. Bonchev St., Bl. 103B

Author: Erik Vasilev Dimitrov

Dissertation title: Macromolecular Design and Synthetic Strategies for the Preparation of Polymers for Delivery of Biologically Active Substances and Oligonucleotides

The research presented in this dissertation was carried out in the "Polymerization Processes" Laboratory, within the "Macromolecular Engineering" research division at the Institute of Polymers, Bulgarian Academy of Sciences.

Part of the research was conducted within the framework of projects funded by the National Science Fund, as well as under contract ДО1-217/30.11.2018 within the National Scientific Program BioActiveMed – Innovative Low-Toxic Biologically Active Substances for Precision Medicine.

Some of the results were obtained using equipment acquired under contract ДО1-322/2023 within the INFRAMAT project (part of the National Roadmap for Scientific Infrastructure), financially supported by the Ministry of Education and Science of the Republic of Bulgaria.

I would like to express my sincere gratitude to my supervisors, Prof. DSc Stanislav Rangelov and Assoc. Prof. Dr. Natalia Toncheva-Moncheva, for their trust, support, and guidance, both during the preparation of this dissertation and throughout my time at the institute and beyond.

I would like to thank Prof. Petar Petrov for his valuable scientific, strategic, and career advice, which significantly broadened my perspective and helped me make more informed decisions regarding my development.

I express my deep appreciation to Prof. Tsvetanov for his immense support, valuable advice, guidance, and friendly attitude.

I would also like to thank Dr.. Georgi Gergov and Dr. Pavel Bakardzhiev, who directed me toward the institute and introduced me to Prof. Rangelov, thus playing a key role in the beginning of my professional path.

I thank Yavor Hristov, Krum Aleksandrov, Sibela Doleva, and Anna Prancheva for the collaboration, positive energy, and friendship both within and beyond the institute.

I would like to express my sincere gratitude to the entire staff of the Institute of Polymers, BAS, for the friendly environment, support, and atmosphere that turned the institute into my second home.

Finally, I thank my family for their unconditional support, patience, and strength, which they provided in every difficult moment. Their presence has been a constant pillar throughout my journey.

LIST OF ABBREVIATIONS

^{1}H NMR	Proton Nuclear Magnetic Resonance
AFM	Atomic Force Microscopy
AGE	Allyl Glycidyl Ether
AMS	4-(azidomethyl)styrene
ATRP	Atom Transfer Radical Polymerization
CAPA	trade name of poly(ε-caprolactone)
CBD	Canabidiol
Chol	Cholesterol
CMS	4-(chloromethyl)styrene
COSY	2D ^{1}H–^{1}H Correlation Spectroscopy
Cryo-TEM	Cryogenic Transmission Electron Microscopy
D	Diffusion Coefficient
Đ	Dispersity Index
DBCO	Dibenzocyclooctyne
DDP	1,3-didodecyloxypropan-2-ol
D_h	Hydrodynamic diameter
DHP	1,3-dihexadecyloxypropan-2-ol
DLS	Dynamic Light Scattering
DMAP	4-(dimethylamino)pyridine
DMF	*N,N*-dimethylformamide
DMSO	Dimethylsulfoxide
DNA	Deoxyribonucleic acid
DOSY	Diffusion-Ordered Spectroscopy
DPH	1,3-diphenylhexa-1,3,5-triene
DPPC	Dipalmitoylphosphatidylcholine
EDC	1-ethyl-3-(3-dimethylaminopropyl)carbodiimide
EEGE	Ethoxyethyl Glycidyl Ether
EO	Ethylene oxide
ETEGA	Ethoxytriethyleneglycol acrylate
HMBC	Heteronuclear Multiple Bond Correlation
HSQC	Heteronuclear Single Quantum Coherence
hν	Photon energy (light)
iPOx	2-isopropyl-2-oxazoline
kDa	Kilodalton
LCST	Lower Critical Solution Temperature
M_n	Number-average Molar Mass

M_w	Weight-average Molar Mass
MWCO	Molecular Weight Cut-Off
N_{agg}	Aggregation Number
PAA	Poly(acrylic acid)
PAMS	Poly((4-azidomethyl)styrene)
PCL	Poly(ε-caprolactone)
PCMS	Poly((4-chloromethyl)styrene)
PEEGE	Poly(ethoxyethyl glycidyl ether)
PEG	Poly(ethylene glycol)
PEO	Poly(ethylene oxide)
PETEGA	Poly(ethoxytriethyleneglycol acrylate)
PG	Polyglycidol
PiPOx	Poly(2-isopropyl-2-oxazoline)
PMDETA	*N,N,N′,N″,N″*-pentamethyldiethylenetriamine
PPO	Poly(propylene oxide)
PS	Polystyrene
PTBA	Poly(tert-butyl acrylate)
R_g	Radius of Gyration
R_h	Hydrodynamic Radius
ssODN	Single-stranded Oligodeoxynucleotide
TEA	Triethylamine
TEM	Transmission Electron Microscopy
TFA	Trifluoroacetic acid
THF	Tetrahydrofuran
UV-Vis	Ultraviolet–Visible spectroscopy
ζ-потенциал	Zeta Potential
ГПХ	Gel-Permeation Chromatography
ЕДТА	Ethylenediaminetetraacetic acid
ИЧ	Infrared Spectroscopy
САС	Critical Assosiation Concentration
СМС	Critical Micelle Concentration
СНК	Spherical Nucleic Acid, SNA

INTRODUCTION

Polymeric nanocarriers represent one of the most active and rapidly developing fields in chemistry and biomedicine over the past two decades. The main reason for this is their high potential to modify the pharmacokinetic and pharmacodynamic profiles of many therapeutic agents, as well as to enable the development of new ones, particularly for applications in gene therapy. The preparation of novel types of nanocarriers often requires polymers with precisely defined molar mass, topology, and composition. This necessitates the development of synthetic strategies comprising various polymerization techniques, functionalization reactions, and conjugation of individual polymer chains in order to obtain the desired product.

Amphiphilic block copolymers with specific architectures are most commonly used for the preparation of such nanocarriers. Different polymerization methods, as well as post-polymerization modifications, enable the synthesis of "smart" materials with predetermined properties that can respond differently depending on the surrounding environment. Today, polymers are known whose behavior changes in response to variations in temperature, pH, light, magnetic fields, redox potential, and other stimuli. The combination of two or more such polymers enables the creation of macromolecules capable of performing complex functions in living biological systems. One particularly promising application of such materials is in the treatment of oncological and genetic diseases. Therefore, their development is of key importance for the advancement of polymer and biomedical sciences.

Two principal approaches are employed in the synthesis of such macromolecules: the use of macroinitiators and the coupling of two or more individual blocks. In the first approach, the synthesis begins with a polymerization that forms one block of the polymer, followed by appropriate end-group functionalization so that polymerization of another monomer can be initiated from these sites to generate the subsequent block. In the second approach, the two blocks are synthesized through two separate polymerization reactions, after which their chain ends are modified with functional groups capable of reacting with each other upon mixing the two polymers, thereby linking them through stable covalent bonds. With the growing popularity of *click* chemistry, the second approach has become particularly widely applied, as it allows the preparation of polymers in which the reactions required to synthesize one block would not be compatible with the presence of the other. This method is especially preferred for the conjugation of polymers with biomolecules such as proteins and nucleic acids, since the latter are often unstable under conditions different from physiological ones. In this way, synthetic nucleolipids, glycolipids, glycoproteins, and other macromolecules can be designed to modulate various biological processes at the cellular and biochemical levels.

Evidence of the enormous importance of macromolecular design is provided by the numerous pharmaceutical products containing polymers that are currently available and actively used in the treatment of major groups of diseases. Pegaspargase (marketed under the trade name Oncaspar®) is a PEGylated form of the enzyme asparaginase and is widely used in the treatment of acute lymphoblastic leukemia. In addition, numerous PEGylated therapeutics are available on the market, including insulin (Peglispro), antihemophilic factor VII (Esperoct), interferons

(Pegintron), and others. An increasing number of drug formulations based on drug-loaded micelles allow the intravenous administration of highly hydrophobic substances in aqueous solutions, significantly improving their bioavailability. Genexol® PM (paclitaxel loaded in PEG-PLA micelles) and Nanoxel® M (docetaxel loaded in PEG-PLA micelles) are examples of such formulations. Furthermore, many modern vaccines rely on polymeric nanocarriers loaded with structures characteristic of the virus or bacterium against which immunity is intended to be generated. The most recent example highlighting the importance of polymer nanoscience in this field is the Pfizer COVID-19 vaccine, which consists of viral mRNA encapsulated in a PEG-modified lipid nanoparticle.

All these considerations clearly underline the importance of developing new and more efficient strategies for the synthesis of biocompatible macromolecules that can be used in the design of nanocarriers with the potential to enable new and more effective therapies for socially significant diseases.

AIMS AND OBJECTIVES OF THE DISSERTATION

The aim of the present dissertation is the development and application of synthetic strategies for the preparation and modification of various types of macromolecules with applications in biomedicine as nanocarriers for biologically active substances and/or as vectors for the delivery of nucleic acids.

The main objectives arising from this aim are:

Synthesis and characterization of:

- polymer–lipid conjugates for surface modification of membranes through the combination of different polymerization techniques with azide–alkyne *click* chemistry;
- nucleolipids obtained via highly efficient *click* chemistry reactions, used for the preparation of a novel type of liposomal spherical nucleic acids;
- polystyrene-based polymers bearing grafted oligonucleotide chains, used for the preparation of spherical nucleic acids with a polymer core;
- linear and star-shaped polyglycidol–poly(ε-caprolactone) copolymers with different compositions and topologies, applicable for the preparation of micellar and niosomal nanocarriers for biologically active substances and drugs.

Investigation of:

- the patterns and specific features of self-assembly and the ability of the synthesized amphiphilic systems to form nanocarriers;
- the physicochemical characteristics and colloidal stability of the obtained nanocarriers;
- the ability of the developed systems to encapsulate and deliver biologically active substances and nucleic acids.

RESULTS AND DISCUSSION

1. Polymer–lipid conjugates

Phospholipids perform a remarkably wide range of functions in living organisms, primarily at the cellular and biochemical levels. In addition to forming the structural basis of the cell membrane, they participate in key processes such as the regulation of membrane permeability and the mediation of cellular recognition processes **[1, 2]**. The development of synthetic organic and polymer chemistry has enabled the preparation of phospholipids and their analogues that do not occur in nature. Through the appropriate selection of functional groups, molar mass, and molecular architecture, it becomes possible to design structures capable of performing functions without analogues in the biological membranes of living organisms. One such example is 1,3-didodecyloxypropan-2-ol (*DDP*), developed in the Polymerization Processes Laboratory, whose structure resembles that of a lipid in which the ester linkages are replaced by ether bonds that are significantly more stable under hydrolytic conditions **[3–9]**. When *DDP* is covalently attached to a hydrophilic polymer (*PEG, PG*), the resulting macromolecules exhibit amphiphilic properties and a tendency toward self-association, enabling the formation and modification of a wide variety of nanostructures **[10–15]**. In the present work, investigations of this class of macromolecules were further extended by replacing *DDP* with 1,3-dihexadecyloxypropan-2-ol (*DHP*), in which the two hydrophobic chains are longer (16 instead of 12 carbon atoms), thus more closely resembling natural lipids. A flexible modular method for the preparation of *DHP*–polymer conjugates via *click* chemistry was developed, allowing the use of polymers synthesized by different polymerization techniques rather than only those obtained through anionic polymerization, as in previous studies. The obtained macromolecules not only exhibit amphiphilic character and a tendency to form various nanostructures in aqueous solutions through self-assembly, but also serve as effective agents for the surface modification of other structures (liposomes, niosomes, etc.) due to the efficient intercalation of the *DHP* fragment into their membranes.

1.1. Preparation and functionalization of 1,3-dihexadecyloxypropan-2-ol (*DHP*)

DHP was obtained in a single step by adapting a procedure described in the literature for the synthesis of *DDP* **[3]**. The reaction involved acid-catalyzed opening of the oxirane ring of glycidyl hexadecyl ether with 1-hexadecanol in the presence of the Lewis acid $SnCl_4$ (**Fig. 1.1**). The product was characterized by ^{1}H NMR and FTIR spectroscopy. The ^{1}H NMR spectrum of the product is shown in **Fig. 1.2**.

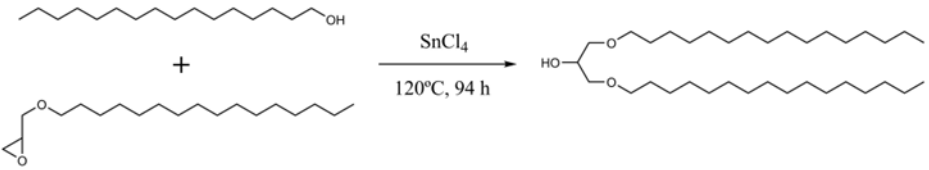

Figure 1.1. Reaction scheme for the synthesis of *DHP*.

The secondary hydroxyl group of *DHP* enables facile modification and the preparation of its derivatives through substitution with various atoms or functional groups. During the course of the investigations, however, it was found that its direct substitution with a nucleophile, even after activation (for example by mesylation), is either impossible or proceeds with unsatisfactory yields. A possible explanation for the observed results can be sought in the reaction mechanism. The substitution reaction is expected to proceed via nucleophilic substitution (Sn), which in most cases occurs through either a unimolecular (Sn1) or a bimolecular (Sn2) mechanism. As is well known, secondary alcohols may react through both mechanisms **[16]**. In the present case, however, unimolecular nucleophilic substitution (Sn1) is highly unfavorable due to

the negative inductive effect of the adjacent oxygen atoms, which would destabilize a hypothetical carbocation intermediate. Bimolecular nucleophilic substitution (Sn2) would also be particularly difficult in this case, owing to the steric shielding of the reaction center by the long hydrocarbon chains, which would hinder a possible backside attack by the azide anion.

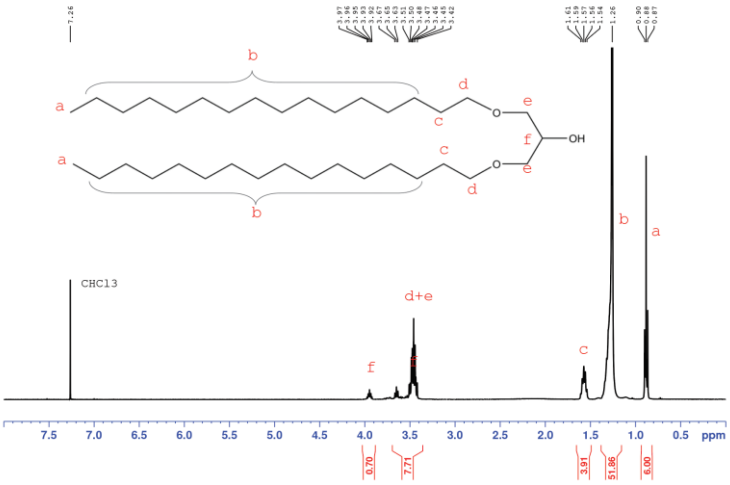

Figure 1.2. ^{1}H NMR spectrum of DHP in $CDCl_3$ at 600 MHz.

In order to introduce suitable functionality without direct substitution of the hydroxyl group, an approach involving its esterification with appropriately substituted carboxylic acids was employed (**Fig. 1.3**). Esterification with *5-hexynoic acid* in the presence of EDC/DMAP resulted in the formation of alkyne-functionalized *DHP*, whereas esterification with 2-bromoisobutyryl bromide, followed by substitution of the bromine atom with sodium azide, yielded azide-functionalized *DHP*.

The ^{1}H NMR and FTIR spectra of the products are presented in **Fig. 1.4**, **Fig. 1.5**, and **Fig. 1.6**, respectively. In this way, the obtained derivatives can participate in azide–alkyne cycloaddition reactions with azide- or alkyne-functionalized polymers, leading to the formation of amphiphilic polymer–lipid conjugates.

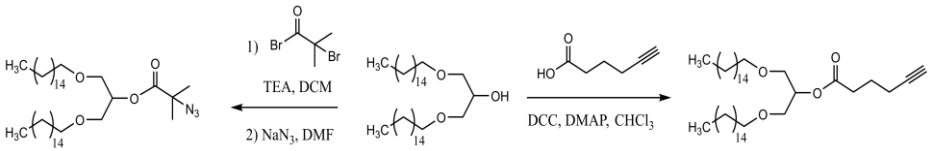

Figure 1.3. Reaction scheme illustrating the functionalization reactions of *DHP*.

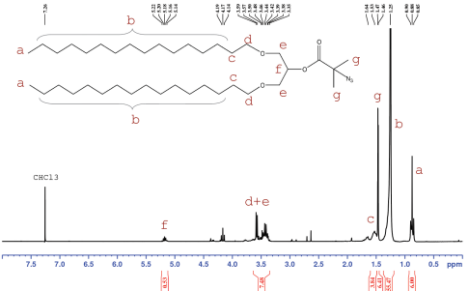

Figure 1.4. ^{1}H NMR spectrum of *DHP-N₃* in $CDCl_3$ at 600 MHz.

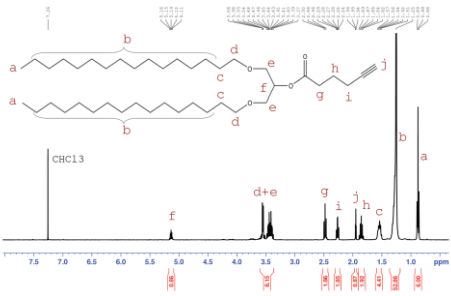

Figure 1.5. ^{1}H NMR spectrum of *DHP-hexynoate* in $CDCl_3$ at 600 MHz.

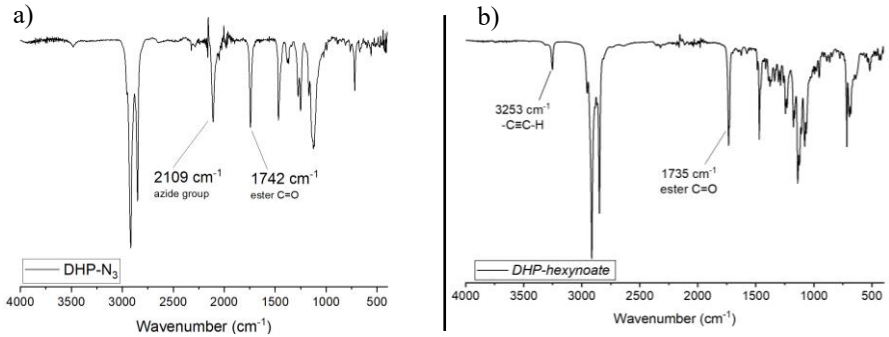

Figure 1.6. FTIR spectra of *DHP-N₃* (a) and DHP-hexynoate (b).

1.2. Preparation of functionalized linear polymers

A series of appropriately functionalized linear polymers was synthesized by different polymerization techniques in order to be conjugated with the functionalized *DHP*. The polymers included *PG, PEG, PiPOx, PTBA,* and *PETEGA*.

1.2.1. Preparation of alkyne-terminated protected polyglycidol (*t-Bu-PEEGE$_{25}$-block-PPO$_4$-OOC(CH$_2$)$_2$C≡CH*)

For the preparation of the polyglycidol segment of the conjugate, "living" anionic polymerization of protected glycidol – ethoxyethyl glycidyl ether (*EEGE*) – was employed. It is well known from the literature that the hydroxyl group in the glycidol molecule reacts during attempts at its polymerization, resulting in poorly defined branched oligomeric products with broad molar mass distributions **[17]**. In order to obtain linear polyglycidol, the hydroxyl group of the monomer must be protected prior to polymerization through reaction with vinyl ethyl ether, whereby it is converted into an acetal. Acetals are stable under basic conditions such as those of anionic polymerization, making the ethoxyethyl group suitable for protecting the monomer.

The polymerization of ethoxyethyl glycidyl ether was initiated with potassium *tert*-butoxide and carried out in DMSO at 60 °C for 14 days. ^{1}H NMR analysis of a sample taken from the reaction on day 14 showed the absence of oxirane protons in the region 2.5–3.2 ppm, indicating quantitative conversion of the monomer. After lowering the temperature to 40 °C, a small amount of propylene oxide was added to the reaction mixture to form a spacer at the chain end that would facilitate subsequent functionalization. After termination of the polymerization with water, the polymer was isolated by extraction with cyclohexane and

characterized by ^{1}H NMR, FTIR, and GPC. GPC showed a monomodal distribution with low dispersity (a chromatogram of the esterified polymer is presented in **Fig. 1.18** below). M_n and the degree of polymerization of the product (**Table 1**) were determined by ^{1}H NMR after deprotection of a small portion of the product. The reaction scheme of the performed reactions is presented in **Fig. 1.7**.

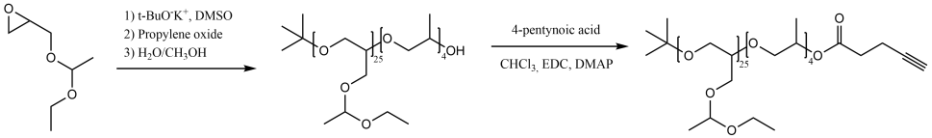

Figure 1.7. Reaction scheme illustrating the synthesis of *t-Bu-PEEGE$_{25}$-block-PPO$_4$-OOC(CH$_2$)$_2$C≡CH*.

The preparation of the alkyne-functionalized PEEGE polymer (*t-Bu-PEEGE$_{25}$-block-PPO$_4$-OOC(CH$_2$)$_2$C≡CH*) was accomplished through esterification of the –OH-terminated precursor with 4-pentynoic acid (**Fig. 1.7**). The reaction was carried out in chloroform, using the EDC/DMAP system as the condensation agent. The presence of a PPO spacer is necessary because otherwise the esterification does not proceed quantitatively **[18]**. In the present case, a polymer with fully esterified chains was obtained, as evidenced by the ratio between the integrals of the signals at 2.5 and 2.3 ppm, corresponding to the protons of 4-pentynoic acid, and those at 4.65 ppm, corresponding to the methine protons of the monomeric units (**Fig. 1.8**). The FTIR spectrum, as expected, showed the presence of a terminal triple bond as well as an ester carbonyl group at 1730 cm^{-1}, further supporting the results of the ^{1}H NMR analysis.

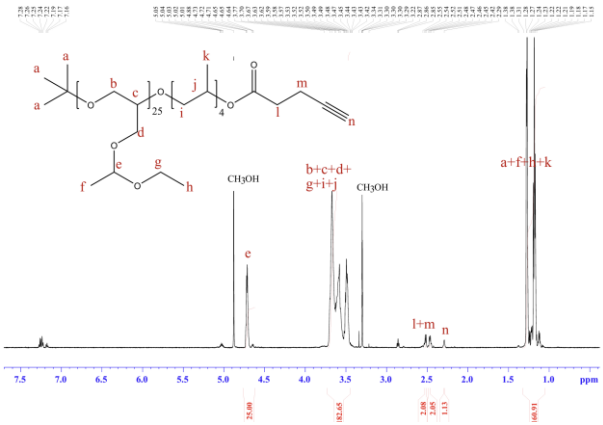

Figure 1.8. ^{1}H NMR spectrum of *t-Bu-PEEGE$_{25}$-block-PPO$_4$-OOC(CH$_2$)$_2$C≡CH* in $CDCl_3$ at 600 MHz.

1.2.2. Preparation of *CH$_3$-PEG$_{68}$-N$_3$*

Commercial PEG 3000 monomethyl ether (*CH$_3$-PEG$_{68}$-OH*) was functionalized with an azide group in two steps. The first step consisted of esterification of the terminal –OH group with mesyl chloride, after which the resulting mesylate was substituted through reaction with sodium azide. The FTIR spectrum of the final product showed the expected changes corresponding to the performed transformations, namely the disappearance of the broad absorption band corresponding to the stretching vibration of the hydroxyl group at 3300 cm^{-1} and the appearance of an absorption band at 2100 cm^{-1} corresponding to the newly introduced azide group (**Fig. 1.9**). Due to the overlap of the signals of the terminal methyl group of the initiator and the

methylene group adjacent to the azide group in the ^{1}H NMR spectrum (**Fig. 1.11**), additional analysis was carried out using HSQC (**Fig. 1.10**). HSQC (*Heteronuclear Single Quantum Coherence*) is a two-dimensional NMR experiment that reveals correlations between protons (^{1}H) and directly bonded heteronuclei (most commonly ^{13}C) through one-bond couplings (^{1}J). The method allows differentiation of functionalities whose chemical shifts overlap in the proton spectrum. As shown in **Fig. 1.10**, the two functionalities of CH_3-PEG_{68}-N_3 (CH_3O– and $–CH_2–N_3$) are clearly distinguished, while signals corresponding to the precursor molecules ($–CH_2–OH$ and $–CH_2–OSO_2CH_3$) are absent, demonstrating the quantitative conversion of the hydroxyl group into an azide group.

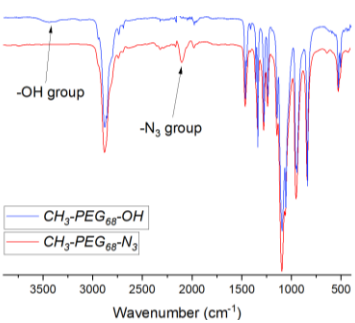

Figure 1.9. FTIR spectra of *CH_3-PEG_{68}-OH* and *CH_3-PEG_{68}-N_3*.

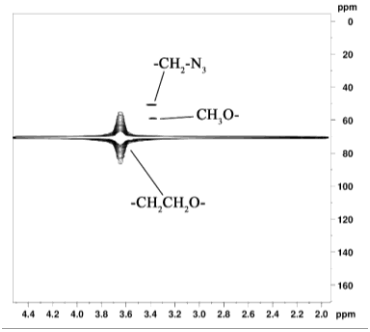

Figure 1.9. FTIR spectra of *CH_3-PEG_{68}-OH* and *CH_3-PEG_{68}-N_3*.

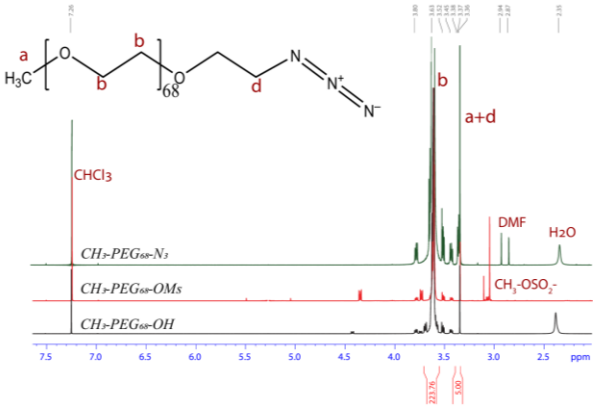

Figure 1.11. ^{1}H NMR spectra of *CH_3-PEG_{68}-OH, CH_3-PEG_{68}-OMs,* and *CH_3-PEG_{68}-N_3* in $CDCl_3$ at 600 MHz. The indicated integral ratios correspond to *CH_3-PEG_{68}-N_3*.

1.2.3. Preparation of *CH₃-PiPOx₂₂-N₃*

Azide-terminated poly(2-isopropyl-2-oxazoline) (*CH₃-PiPOx₂₂-N₃*) was synthesized via cationic ring-opening polymerization of 2-isopropyl-2-oxazoline. The monomer was obtained through a reaction between isobutyric acid and ethanolamine at 230 °C. Its characterization was carried out by FTIR and ^{1}H NMR spectroscopy, as well as by gas chromatography.

Polymerization of the obtained monomer was performed in acetonitrile using methyl tosylate as the initiator at 80 °C in a sealed vessel. After completion of the reaction time, termination was achieved by adding an excess of solid sodium azide and allowing the mixture to stand at room temperature for 24 h. In this way, a polymer bearing an azide group directly at the chain end was obtained. Removal of unreacted sodium azide and monomer was accomplished by ultrafiltration in water through a 1 kDa MWCO membrane. The final product exhibited a monomodal molar mass distribution and a low dispersity in GPC (**Fig. 1.23** below). The degree of polymerization, corresponding to 22 monomer units, was calculated based on the integral ratio between the signal of the methyl group from the initiator at 3.07 ppm and the signals of the remaining protons of the monomer units in the ^{1}H NMR spectrum (**Fig. 1.12**). The molar mass characteristics of the polymer are summarized in **Table 1**.

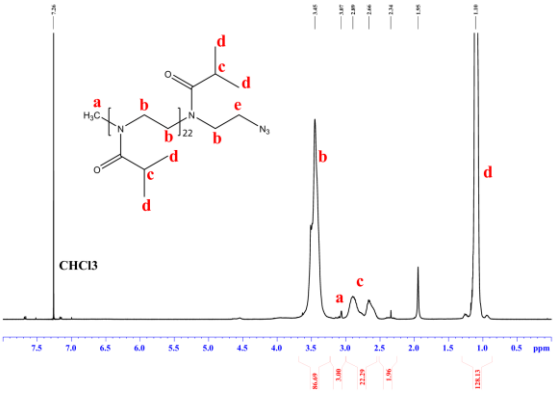

Figure 1.12. ^{1}H NMR spectrum of *CH₃-PiPOx₂₂-N₃* in $CDCl_3$ at 600 MHz.

1.2.4. Preparation of azide-terminated *poly(tert-butyl acrylate)* (*PTBA₃₅-N₃*)

Poly(*tert*-butyl acrylate) (PTBA₃₅-Br) was synthesized via ATRP polymerization of *tert*-butyl acrylate. Ethyl 2-bromopropionate was used as the initiator, and the reaction was catalyzed by CuBr and PMDETA. The obtained polymer exhibited a monomodal molar mass distribution and low dispersity according to GPC analysis (see **Fig. 1.25** below). The degree of polymerization and the molar mass of the compound (**Table 1**) were determined from the integral ratio between the methyl group of the initiator at 1.10 ppm and the methine protons of the monomer units at 2.21 ppm in the ^{1}H NMR spectrum (**Fig. 1.13**).

Since under the conditions of ATRP polymerization the resulting polymer contains bromine at the chain end, its functionalization with an azide group was easily achieved in a single step through reaction of the polymer with an excess of sodium azide in DMF. Successful functionalization is evidenced by the appearance of a peak at 2109 cm^{-1} in the FTIR spectrum, corresponding to the azide group (**Fig. 1.14**).

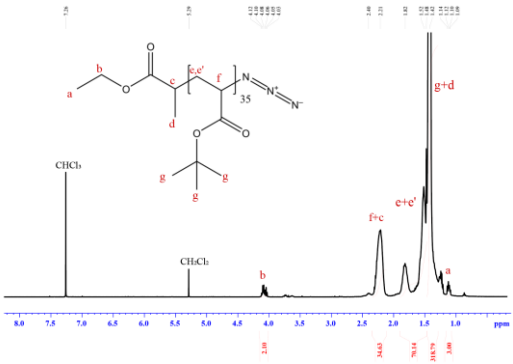

Figure 1.13. ^{1}H NMR spectrum of *PTBA$_{35}$-N$_3$* in $CDCl_3$ at 600 MHz.

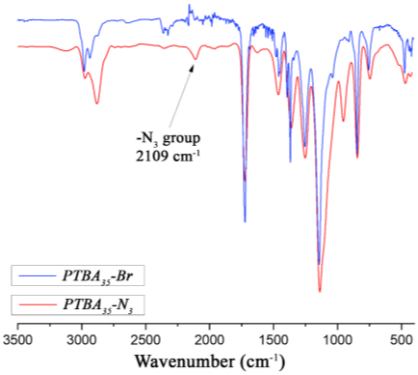

Figure 1.14. FTIR spectra of *PTBA$_{35}$-Br* and *PTBA$_{35}$-N$_3$*.

1.2.5. Preparation of azide-terminated *poly(ethoxytriethylene glycol acrylate) (PETEGA$_{13}$-N$_3$)*

The monomer ethoxytriethylene glycol acrylate (*ETEGA*) was obtained by esterification of triethylene glycol monoethyl ether with acryloyl chloride. The resulting ester was isolated from the reaction mixture by extraction and purified by column chromatography.

ETEGA was polymerized via controlled radical polymerization, in this case ATRP. Similarly to *tert*-butyl acrylate, ethyl 2-bromopropionate was used as the initiator and the CuBr/PMDETA system as the catalyst. GPC analysis showed a monomodal molar mass distribution and low dispersity of the obtained polymer, while ^{1}H NMR spectroscopy indicated a degree of polymerization corresponding to 13 monomer units (**Fig. 1.15**, **Fig. 1.27** below, **Table 1**).

The preparation of *PETEGA$_{13}$-N$_3$* was accomplished through nucleophilic substitution of the terminal bromine atom with an excess of sodium azide. The FTIR spectrum of the obtained product showed a peak at 2108 cm^{-1} corresponding to the stretching vibration of the azide group (**Fig. 1.16**).

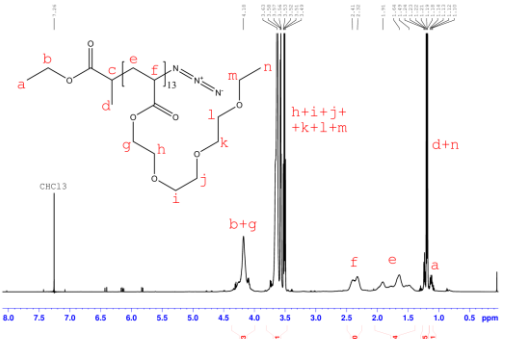

Figure 1.15. ^{1}H NMR spectrum of *PETEGA$_{13}$-N$_3$* in $CDCl_3$ at 600 MHz.

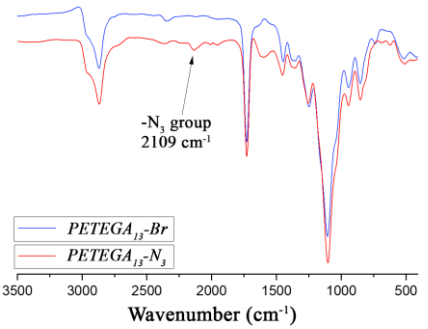

Figure 1.16. FTIR spectra of *PETEGA$_{13}$-Br* and *PETEGA$_{13}$-N$_3$*.

As shown in **Table 1**, the molar masses of the polymers that do not contain protected functional groups (*CH_3-PEG_{68}-N_3, CH_3-$PiPOx_{22}$-N_3, and $PETEGA_{13}$-N_3*) are similar, falling within the range of 2200–3200 g/mol. The molar masses of the other two polymers, which contain protected groups (*t-Bu-$PEEGE_{25}$-block-PPO_4-$OOC(CH_2)_2C{\equiv}CH$ and $PTBA_{35}$-N_3*), are higher; however, after their deprotection, their molar masses again fall within the same range (2250 and 2660 g/mol, respectively). Due to the different molar masses of the monomer units composing them, the five polymers exhibit different degrees of polymerization and consequently different side-chain lengths. This is also one of the factors responsible for the different behavior and properties of the resulting lipid–polymer conjugates during self-assembly (see below).

Polymer	Degree of polymerization (ЯМР)	$M_{n(NMR)}$ (g/mol)	$M_{n(GPC)}$ (g/mol)	$M_{w(GPC)}$ (g/mol)	*Đ*
t-Bu-$PEEGE_{25}$-блок-PPO_4-$OOC(CH_2)_2C{\equiv}CH$	25	4050	3490	4050	1.16
CH_3-PEG_{68}-N_3	68	3030	2980	3230	1.08
CH_3-$PiPOx_{22}$-N_3	22	2540	2740	3530	1.29
$PTBA_{35}$-N_3	35	4630	6340	7530	1.19
$PETEGA_{13}$-N_3	13	3180	3800	4870	1.28

Table 1. Molar mass characteristics of the synthesized polymers.

1.3. Preparation of polymer–lipid conjugates

The functionalized polymers and DHP were used for the preparation of amphiphilic macromolecules consisting of a hydrophilic polymer block and a hydrophobic lipid-like moiety. Chemical coupling of the precursors was carried out via azide–alkyne cycloaddition reactions, and in the cases of *DHP–PG* and *DHP–PAA* the *click* reaction was followed by deprotection of the protected functional groups. A general scheme illustrating the described transformations is presented in **Fig. 1.17**.

Figure 1.17. Schematic representation of the click reaction between *DHP* and the polymers.

1.3.1. Preparation of polyglycidol–lipid conjugate (*DHP–PG*)

The coupling of *t-Bu-$PEEGE_{25}$-block-PPO_4-$OOC(CH_2)_2C{\equiv}CH$* with *DHP–N_3* was carried out via a copper-catalyzed azide–alkyne *click* reaction. The reaction was performed in an excess of *DHP* in THF at 40 °C, using PMDETA as the ligand. After completion of the reaction, the copper complex was removed by column chromatography (aluminum oxide/THF), and the excess *DHP* was removed by dialysis through a 1 kDa MWCO cellulose membrane in a methanol:water mixture (9:1). The final product was characterized by GPC and ^{1}H NMR spectroscopy (**Fig. 1.18** and **Fig. 1.19**). As shown in **Fig. 1.18**, the GPC analysis demonstrates a clear shift of the curve toward lower elution times, corresponding to an increase in hydrodynamic volume and, consequently, molar mass. In the ^{1}H NMR spectrum, a new signal appears at 7.6 ppm, corresponding to a proton of the newly formed triazole ring (**Fig. 1.19**).

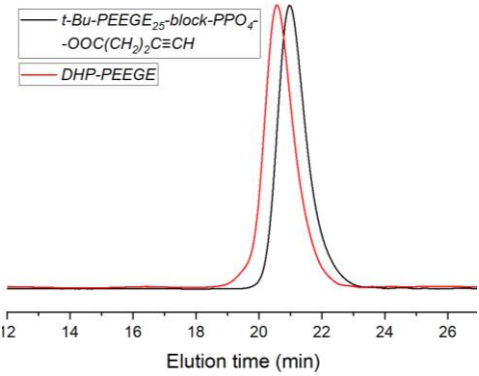

Figure 1.18. GPC chromatograms of *t-Bu-PEEGE$_{25}$-block-PPO$_4$-OOC(CH$_2$)$_2$C≡CH* and *DHP-PEEGE*.

The final stage of the conjugate synthesis consisted of the removal of the protective ethoxyethyl groups from the glycidol monomer units. This was accomplished by reaction with methanol in the presence of catalytic amounts of $AlCl_3.6H_2O$. Complete deprotection of the compound was confirmed by ^1H NMR spectroscopy. As shown in **Fig. 1.19**, the integral ratios of the signals at 1.2 and 3.5 ppm relative to the remaining signals in the spectrum decrease significantly. In addition, a new signal appears at 4.55 ppm (protons from the –OH group), at the expense of the disappearing signal at 4.75 ppm (methine protons of the protecting group), which clearly indicates successful deprotection of the polymer.

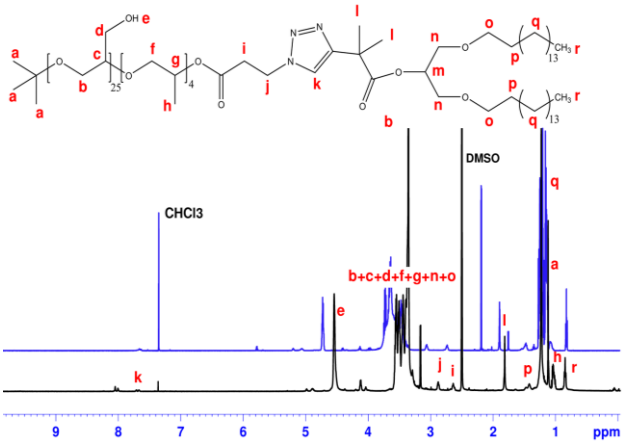

Figure 1.19. ^1H NMR spectra of *DHP-PEEGE* in $CDCl_3$ (blue) and *DHP-PG* in DMSO-d_6 (black) at 600 MHz.

1.3.2. Preparation of polyethylene glycol–lipid conjugate (*DHP–PEG*)

The coupling of *CH$_3$-PEG$_{68}$-N$_3$* with *DHP-hexynoate* was carried out via a copper-catalyzed azide–alkyne *click* reaction. The reaction was performed in THF at 40 °C. Removal of the catalyst was achieved by ultrafiltration in water through a 1 kDa MWCO membrane in the presence of the disodium

salt of EDTA, which forms a stable complex with copper ions. Removal of unreacted *DHP* was accomplished by reprecipitation of the lyophilizate obtained after ultrafiltration in cold diethyl ether. Successful conjugation was confirmed by the decrease in elution time observed in GPC (**Fig. 1.20**) and by the appearance of new signals at 7.73, 4.56, and 3.90 ppm in the ^{1}H NMR spectrum (**Fig. 1.21**).

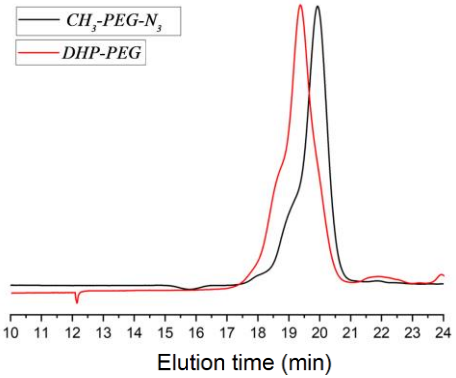

Figure 1.20. GPC chromatograms of *CH₃-PEG₆₈-N₃* and *DHP-PEG*.

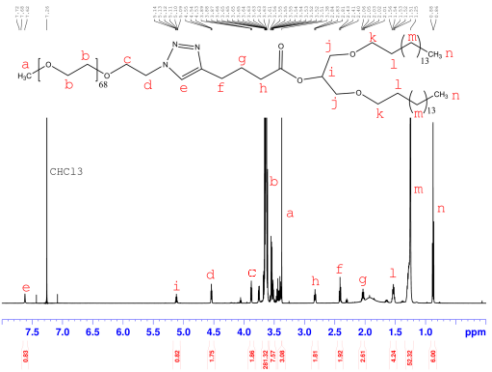

Figure 1.21. ^{1}H NMR spectrum of *DHP-PEG* in $CDCl_3$ at 600 MHz.

1.3.3. Preparation of poly(2-isopropyl-2-oxazoline)–lipid conjugate (*DHP–PiPOx*)

The conjugation of *CH₃-PiPOx₂₂-N₃* with *DHP-hexynoate* was carried out analogously to the preparation of *DHP–PEG*. In this case, however, the thermoresponsive properties of PiPOx, which are retained in its conjugate with *DHP*, were utilized for isolation. At temperatures below 35 °C (**Fig. 1.22**), all components of the reaction mixture, except the excess *DHP-hexynoate*, were completely soluble in water, which allowed removal of the latter. At temperatures above 35 °C, *DHP–PiPOx* precipitates as a white solid, enabling its isolation by centrifugation at 40 °C.

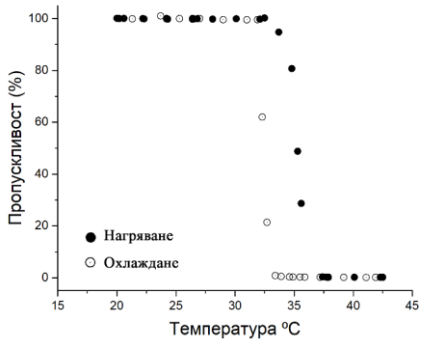

Figure 1.22. LCST of *DHP-PiPOx* determined by UV–Vis transmittance at 500 nm and a concentration of 1 mg/mL.

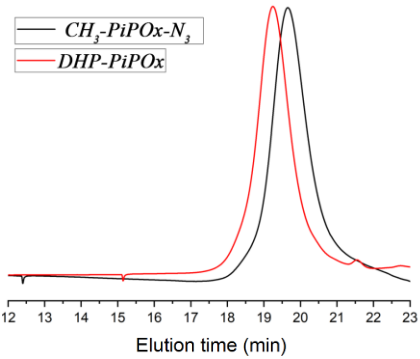

Figure 1.23. GPC chromatograms of *CH₃-PiPOx₂₂-N₃* and *DHP-PiPOx*.

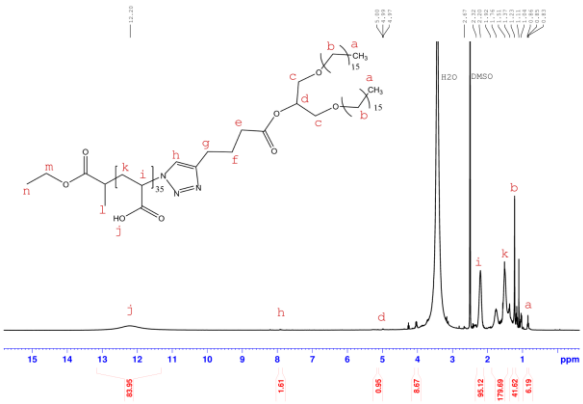

Figure 1.26. ^{1}H NMR spectrum of *DHP-PAA* in DMSO-d_6 at 600 MHz.

The final product was characterized by ^{1}H NMR spectroscopy and GPC. Similarly to the other conjugates, a clear decrease in the retention time in GPC was observed (**Fig. 1.23**), as well as the appearance of new signals at 7.61, 4.67, and 3.88 ppm in the ^{1}H NMR spectrum, corresponding to a proton of the triazole ring and to the terminal methylene groups of the polymer adjacent to the triazole ring (**Fig. 1.24**).

1.3.4. Preparation of a lipid conjugate (*DHP–PAA*) of poly(acrylic acid)

The preparation of DHP-functionalized poly(acrylic acid) was accomplished through a *click* reaction between *DHP-hexynoate* and *PTBA$_{35}$-N$_3$*, catalyzed by Cu(I), followed by deprotection of the *tert*-butyl protecting groups. Purification of the product from the *click* reaction (*DHP–PTBA*) was carried out by column chromatography (silica gel/THF), and confirmation of its structure was achieved by ^{1}H NMR spectroscopy and GPC. In the GPC analysis, a decrease in retention time corresponding to an increase in molar mass was observed (**Fig. 1.25**), while in the ^{1}H NMR spectrum a signal at 7.58 ppm was detected, corresponding to the proton attached to the nitrogen atom of the triazole ring.

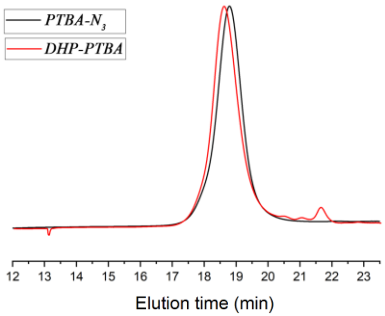

Figure 1.25. GPC chromatograms of *PTBA$_{35}$-N$_3$* and *DHP-PTBA*.

To obtain a conjugate of DHP with poly(acrylic acid), the *tert*-butyl groups of *DHP–PTBA* were hydrolyzed through reaction with trifluoroacetic acid in dichloromethane. The product was isolated by evaporation to dryness under reduced pressure. The ^{1}H NMR spectrum showed the disappearance of the intense signal at 1.4 ppm corresponding to the *tert*-butyl ester groups (**Fig. 1.26**). This, together with the

changed solubility of the compound (it became soluble in polar solvents and water), indicates the successful hydrolysis of the ester groups of poly(*tert*-butyl acrylate).

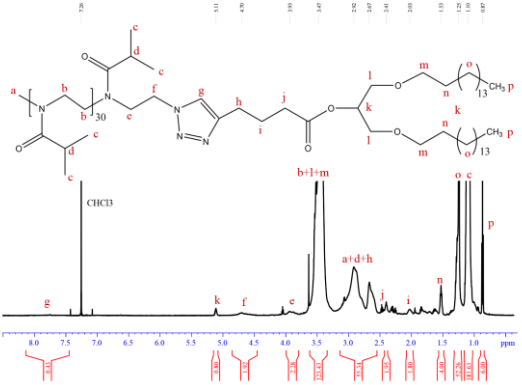

Figure 1.24. ^{1}H NMR spectrum of *DHP-PiPOx* in $CDCl_3$ at 600 MHz.

1.3.5. Preparation of poly(ethoxytriethylene glycol acrylate)–lipid conjugate (*DHP–PETEGA*)

The coupling of *PETEGA$_{13}$-N$_3$* with *DHP-hexynoate* was also carried out via copper-catalyzed azide–alkyne cycloaddition. Successful completion of the reaction required the use of a large excess of *DHP-hexynoate*, which, however, proved particularly difficult to separate from the product at the end of the reaction. To achieve this, an alkyne-scavenging resin was synthesized via radical copolymerization of (4-chloromethyl)styrene with divinylbenzene. The obtained resin was treated with an excess of sodium azide in DMF, resulting in the conversion of the pendant chloromethyl groups of the gel into azidomethyl groups.

The resulting resin is completely insoluble in all solvents but simultaneously contains a large number of free azide groups on its surface, which under suitable conditions can react with terminal alkynes. Once reacted, the alkyne becomes firmly attached to the surface of the resin and can be easily removed from the reaction mixture by filtration.

This approach enabled efficient and selective removal of the excess *DHP-hexynoate* within a one-pot process. After completion of the *click* reaction with *PETEGA$_{13}$-N$_3$*, an excess of the azide-functionalized resin was added to the mixture, and the reaction was allowed to proceed for an additional 24 h under the same conditions. Subsequently, the captured *DHP-hexynoate* was removed by filtration together with the resin, while the copper complex was removed by column chromatography (silica gel/THF).

The final product exhibited a shift toward shorter retention time in GPC compared to the starting polymer (**Fig. 1.27**) and showed the expected integral ratios in the ^{1}H NMR spectrum (**Fig. 1.28**).

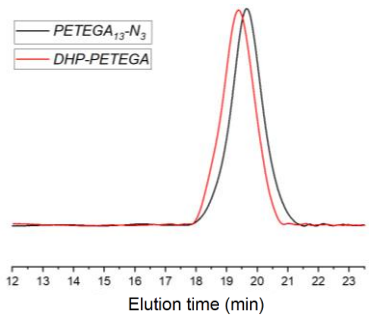

Figure 1.27. GPC chromatograms of *PETEGA$_{13}$-N$_3$* and *DHP-PETEGA*.

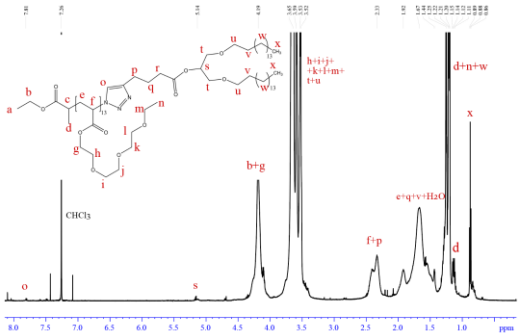

Figure 1.28. ^{1}H NMR spectrum of *DHP-PETEGA* in $CDCl_3$ at 600 MHz.

1.4. Characteristics of polymer–lipid conjugates

An efficient modular synthetic strategy for the preparation of polymer–lipid conjugates via azide–alkyne *click* chemistry with different types of polymer blocks was developed. The method allows installation of an azide group on the lipid mimetic and a terminal alkyne at the end of the polymer chain, or vice versa, thereby providing flexibility for its application to polymers obtained by different polymerization techniques. For example, the direct preparation of azide-terminated poly(oxazoline)s is possible through termination of the polymerization with sodium azide, whereas, due to the specific reactivity of the terminal –OH group, esterification with an alkynoacid acid is more suitable in the case of *PEEGE*. The strategy is compatible with a wide range of protecting groups within the polymer chain due to the mild conditions of the *click* reaction and the stability of the covalent bonds through which the two molecules are connected. In the present work, ethoxyethyl acetal protection and *tert*-butyl ester protection were used in two of the polymer blocks, respectively, and their presence did not create any difficulties in carrying out the reactions.

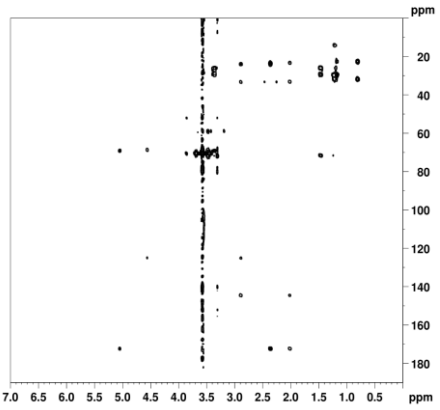

Figure 1.29. HMBC spectrum of *DHP-PEG*.

The molar mass characteristics of the polymer–lipid conjugates were determined by GPC and ^{1}H NMR (**Table 2**). Additional two-dimensional NMR experiments (COSY, HSQC, HMBC, DOSY) confirmed the covalent coupling of the macromolecules. The HMBC spectrum of *DHP–PEG* is presented in **Fig. 1.29**. The observed cross-correlation signals (δ_H/δ_C 4.56/125.56; 4.56/68.59; 2.9/144.62; 2.9/125.56; 2.02/144.62 ppm) unequivocally confirm the coupling of DHP with PEG through a triazole ring.

The coupling of the lipid mimetic with the polymers is particularly well illustrated by monitoring the diffusion coefficients of the molecules using Diffusion-Ordered Spectroscopy (DOSY). The two-dimensional DOSY spectra of *DHP-hexynoate*, *CH$_3$-PEG$_{68}$-N$_3$*, and *DHP–PEG* are presented in **Fig. 1.30**. A clear decrease in the diffusion coefficient is observed for the conjugate *DHP–PEG* compared with that of the precursor molecules from which it was obtained, which can be explained by the increase in molar mass and,

consequently, the successful *click* reaction. The diffusion coefficients of the remaining polymer–lipid conjugates are summarized in **Table 3**.

Compound	M_{nGPC} g/mol	M_{wGPC} g/mol	M_{nGPC} g/mol	*Đ* (GPC)
DHP-PEEGE	4260	5420	4410	1.27
DHP-PG	-	-	2600	-
DHP-PEG	4430	5470	3670	1.23
DHP-PiPOx	4300	5080	4090	1.18
DHP-PTBA	6140	7600	5270	1.24
DHP-PAA	-	-	3300	-
DHP-PETEGA	4220	5170	3810	1.22

Table 2. Molar mass characteristics of the obtained polymer–lipid conjugates.

The obtained macromolecular products exhibit a pronounced amphiphilic character, as the two hydrocarbon chains in their hydrophobic fragment structurally resemble those found in phospholipids. This determines the potential of the studied molecules for application in the preparation of nanostructures, as well as for the modification of phospholipid and polymer membranes of various nanocarriers, thereby altering their properties or imparting new functionalities.

The behavior of the obtained *DHP*–polymer conjugates in aqueous solution was investigated in order to evaluate their potential for self-organization and the formation of nanostructures. The critical association concentrations (CAC) were determined using the pyrene solubilization method. It was established that at low concentrations the molecules are present in solution as unimers, whereas with increasing concentration a gradual formation of hydrophobic domains is observed, indicating self-association into nanostructures. Unlike classical low-molecular-weight surfactants, the transition from the unimeric to the aggregated state in *DHP*–polymer conjugates occurs over a broad concentration range, reflecting the lower cooperativity of the self-association process (**Fig. 1.31**). The nature and width of this transition depend on the type, length, and architecture of the polymer chain attached to the lipid-mimetic fragment. The critical association concentrations exhibit relatively low values (**Table 4**), indicating that the aggregates remain stable upon dilution.

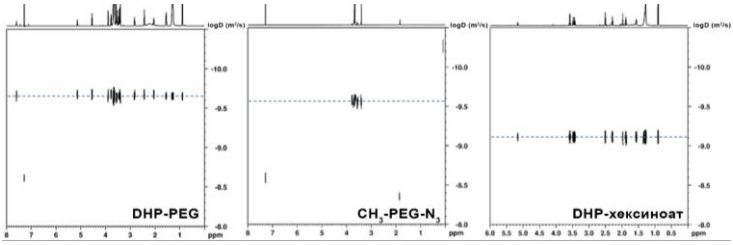

Figure 1.30. DOSY spectra of *DHP-PEG* and the precursor molecules from which it was obtained.

Compound	D [$m^2.s^{-1}$]	D conjugate [$m^2.s^{-1}$]	
		D^{DHP}	$D^{polymer}$
DHP-хексиноат	5.87 x 10^{-10}		
CH_3-PEG_{68}-N_3	2.43 x 10^{-10}		
CH_3-$PiPOx_{22}$-N_3	2.50 x 10^{-10}		
DHP-PEG		1.99 x 10^{-10}	1.99 x 10^{-10}
DHP-PG		7.54 x 10^{-11}	7.48 x 10^{-11}
DHP-PAA		5.17 x 10^{-11}	4.73 x 10^{-11}
DHP-PiPOx		2.52 x 10^{-10}	2.18 x 10^{-10}
DHP-PETEGA		Monoexponential approximation: 4.56 x 10^{-10}	Monoexponential approximation: 2.39 x 10^{-10}
		Biexponential approximation: 2.3 x 10^{-10} and 6.2 x 10^{-10}	Biexponential approximation: 1.96 x 10^{-10} and 3.64 x 10^{-10}

Table 3. Translational diffusion coefficients (D) of *DHP-hexynoate*, selected polymers, and the obtained conjugates determined by DOSY.

Dynamic, static, and electrophoretic light scattering were used to characterize the obtained aggregates. It was established that the size, molar mass, and aggregation number of the particles strongly depend on the structure of the polymer component. Depending on the particular conjugate, aggregates with hydrodynamic sizes ranging from tens to hundreds of nanometers were observed. The aggregation number (N_{agg}), and consequently M_w, varied significantly among the different aggregates, which can be attributed to the different nature of the polymer blocks. The ζ-potential exhibited low values for all particles except those obtained from *DHP–PAA*, where the large negative ζ-potential arises from the negatively charged carboxyl groups present in the monomer units of poly(acrylic acid) (**Table 5**). The morphological diversity of the aggregates was directly confirmed by cryogenic transmission electron microscopy (Cryo-TEM), which revealed the presence of spherical and irregular vesicles (*irregular vesicles*), worm-like micelles (*worm-like micelles*), and rod-like structures, as well as the coexistence of different types of nanoparticles depending on the specific *DHP*–polymer conjugate (**Fig. 1.32**). The obtained results are in good agreement with the data from static and dynamic light scattering and highlight the sensitivity of the self-assembly process to the architecture of the macromolecules.

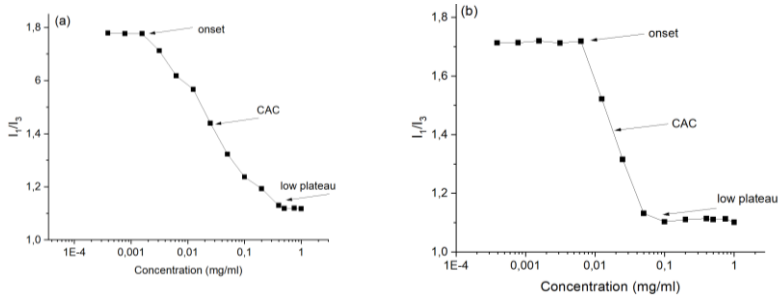

Figure 1.31. Dependence of the I_1/I_3 ratio in the fluorescence spectrum of pyrene in aqueous solutions of (a) *DHP-PG* and (b) *DHP-PAA* at 25 °C.

***DHP*-polymer**	**Temperature**	**Onset (mg/ml)**	**Low plateau (mg/ml)**	**CAC (mg/ml)**
DHP-PEG	25 °C	1.56×10^{-3}	0.2	0.025
	37 °C	6.25×10^{-3}	0.1	0.030
DHP-PG	25 °C	2.10×10^{-3}	0.5	0.025
	37 °C	3.13×10^{-3}	0.5	0.025
DHP-PiPOx	25 °C	3.13×10^{-3}	0.4	0.0125
	37 °C	3.50×10^{-3}	0.2	0.025
DHP-PETEGA	25 °C	6.20×10^{-3}	0.4	0.05
	37 °C	8.50×10^{-3}	0.4	0.06
DHP-PAA	25 °C	6.40×10^{-3}	0.05	0.02
	37 °C	1.50×10^{-2}	0.1	0.03

Table 4. Characteristics of the aggregation behavior of DHP–polymer conjugates measured at 25 °C and 37 °C. *Onset* – concentration at which the I_1/I_3 ratio begins to decrease. *Low plateau* – the lowest concentration at which the I_1/I_3 ratio remains constant. *CAC* – critical aggregation concentration.

***DHP*-polymer**	R_h (nm)	R_g (nm)	R_g/R_h	M_w (10^6 g.mol^{-1})	N_{agg}	ζ (mV)
DHP-PEG	10.0	17.0	1.70	0.471	128	3.99
DHP-PG	145.0	127.0	0.88	81.0	30566	-7.78
DHP-PiPOx	15,0/95.0	84.5	-	6.09	1489	-7.57
DHP-PETEGA	160.0	165.0	1.03	130.0	34120	2.42
DHP-PAA	80.0	113.0	1.41	14.5	4394	-39.0

Table 5. Characteristics of the aggregates obtained from DHP–polymer conjugates in aqueous solution determined by static and dynamic light scattering. R_h – hydrodynamic radius, R_g – radius of gyration, N_{agg} – aggregation number, ζ – zeta potential.

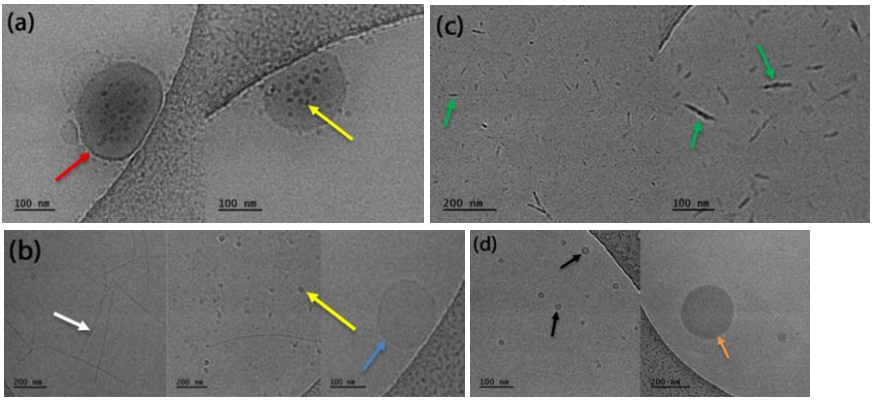

Figure 1.32. Cryo-TEM images of aggregates formed from *DHP-PG* (a), *DHP-PiPOx* (b), *DHP-PAA* (c), and *DHP-PETEGA* (d) in water. Observed structures include spherical vesicles (red arrow), small spherical micelles (yellow arrows), worm-like micelles (white arrow), rod-like micelles (green arrows), small vesicles (black arrows), and membrane-free particles (orange arrow).

2. DHP-functionalized oligonucleotides

Gene therapy is one of the most rapidly developing areas in modern medicine. It represents an approach in which genetic material is introduced, replaced, or modulated within the cells of the body in order to treat or prevent disease. The therapeutic effect is achieved by correcting defective genes, introducing missing functional copies, or regulating the expression of specific genes, with viral or synthetic vectors used for delivery. This strategy targets the molecular "source" of the disease itself and has the potential for long-term or even permanent restoration of impaired biological functions **[19,20]**.

Traditional viral carriers remain highly efficient vectors for gene therapy but are associated with limitations such as immunogenicity, limited cargo capacity, and the risk of viral genome integration into the host genome. For this reason, interest in non-viral platforms has increased significantly over the past two decades. Synthetic polymers, lipid nanoparticles, and hybrid materials allow greater control over the structure, cargo, stability, and release of nucleic acids **[21]**.

In this context, spherical nucleic acids (SNAs) represent a completely new class of architectures in which nucleic acid strands are densely and radially arranged on the surface of a compact core. This three-dimensional configuration confers unique properties not possessed by linear DNA and RNA, including enhanced cellular uptake without the need for additional transfection agents, high structural stability, modular design capability, and excellent colloidal and enzymatic stability. These characteristics make SNAs promising platforms for gene therapy, genome editing, vaccines, and diagnostic systems **[22–24]**.

In the present work, a new type of liposome-based SNA was developed through the intercalation of synthetic nucleolipids obtained via *click* chemistry reactions between suitably functionalized single-stranded DNA oligonucleotides and *DHP*. Two different approaches for the preparation of nucleolipids were demonstrated, both involving direct covalent coupling of the two molecules in the absence of catalysts and metals, which makes the methods particularly attractive for biological applications.

2.1. Preparation of azide- and alkene-functionalized *DHP*

As mentioned in Section **1.1**, direct substitution of the hydroxyl group in the *DHP* molecule did not yield satisfactory results due to the mechanistic characteristics of the reaction. Therefore, an approach was undertaken to "move" the hydroxyl group away from the steric shielding effect of the hydrocarbon chains by installing a poly(ethylene oxide) spacer (**Fig. 1.33**). Initially, the hydroxyl group was deprotonated through reaction with metallic potassium in THF, after which a predetermined amount of liquid ethylene oxide was added while cooling below 0 °C. Due to the physical properties of ethylene oxide (*b.p.* = 10.7 °C), the reaction was carried out in a sealed ampoule at room temperature.

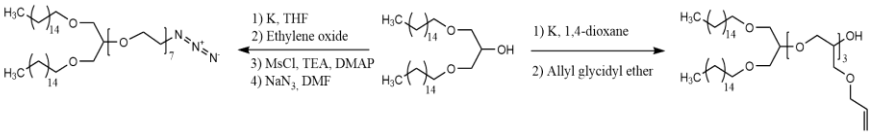

Figure 1.33. Reaction scheme for the synthesis of *DHP-(EO)₇-N₃* and *DHP-AGE₃*.

In the ^{1}H NMR spectrum of the product (**Fig. 1.34**), new signals appear at 3.64 ppm corresponding to the methylene groups of *PEG*. From the ratio of their integral relative to the terminal methyl groups of the alkyl chains of *DHP* at 0.88 ppm, the average degree of polymerization was calculated, corresponding to seven oxyethylene units. With the installation of this spacer, the problem of the low reactivity of the compound toward nucleophiles was resolved, and azidation of the terminal hydroxyl group proceeded smoothly. The NMR spectra of the intermediate and final products are shown in **Fig. 1.34**.

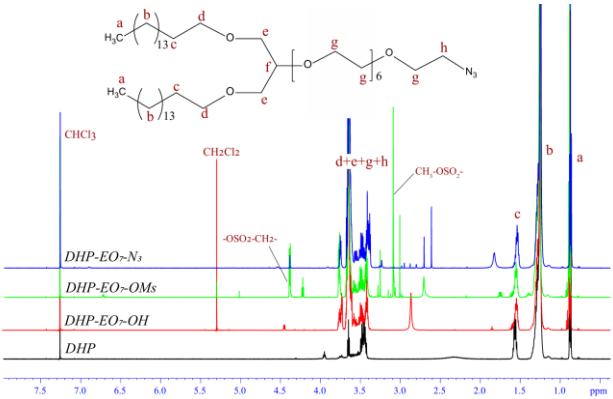

Figure 1.34. ^{1}H NMR spectra of *DHP-(EO)$_7$-N$_3$* and its precursor compounds in $CDCl_3$ at 600 MHz.

The preparation of alkene-functionalized *DHP* was carried out in an analogous manner via anionic polymerization, using allyl glycidyl ether as the monomer. On average, three monomer units were introduced per *DHP* molecule in order to further increase the efficiency of the interaction with thiol groups. This is important because cases of difficult thiol–ene *click* reactions have been reported in the literature when both reactants possess high molar mass **[25]**. In the ^{1}H NMR spectrum of the product (**Fig. 1.35**), the signals at 5.8, 5.23, and 5.03 ppm corresponding to the allyl group are clearly observed. Their integral ratio relative to the methyl groups of *DHP* at 0.92 ppm indicates the presence of an average of three monomer units per *DHP* molecule.

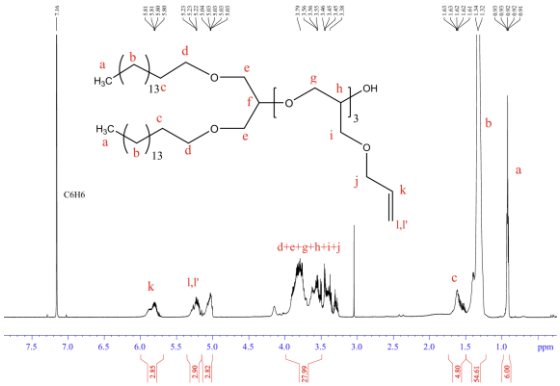

Figure 1.35. ^{1}H NMR spectrum of *DHP-AGE$_3$* in C_6D_6 at 600 MHz.

2.2. Preparation of nucleolipids

The preparation of *DHP*-functionalized nucleic acids was carried out via *click* reactions between *DHP–EO$_7$–N$_3$* or *DHP–AGE$_3$* and appropriately functionalized single-stranded DNA with a nonspecific base sequence (**Table 6**). Depending on the functional groups, two types of *click* reactions were performed: azide–alkyne cycloaddition in the absence of a catalyst and a photoinduced thiol–ene *click* reaction.

Oligonucleotide name	Base sequence 5' → 3'	M_w (g/mol)	Clickable functional group
ThiolC6-oligo	Thiol-C6-spacer 18-ta ata cga ctc act ata gg	6670	**-SH**
DBCO-Oligo	DBCO-$(EO)_4$-spacer 18-ta ata cga ctc act ata gg	6950	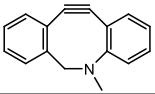

Table 6. Characteristics of the oligonucleotides used.

2.2.1. Conjugation via thiol–ene *click*

The coupling of *DHP–AGE₃* with a thiol-functionalized oligonucleotide was carried out via a UV-induced thiol–ene *click* reaction. To ensure complete conjugation of the oligonucleotide, the reaction was performed in an excess of *DHP–AGE₃*. As a source of monochromatic UV light, a specially designed diode lamp capable of being mounted onto a flask and allowing power regulation was used. The irradiation wavelength was 365 nm, and all photoreactions were carried out at 30 °C.

The reaction time and lamp power were carefully selected so as not to cause degradation of the oligonucleotides. It is well known that under irradiation with low-wavelength UV light, nucleic acids may undergo chemical modifications, the most common of which are the formation of thymidine dimers and photoinduced oxidation **[26]**. In order to determine the permissible irradiation dose at which no structural changes occur in the oligonucleotides, control experiments were performed using a "sacrificial", non-functionalized oligonucleotide. This oligonucleotide was subjected to conditions similar to those used in the reaction, and the changes occurring in its UV spectrum over time were monitored (**Fig. 1.36**).

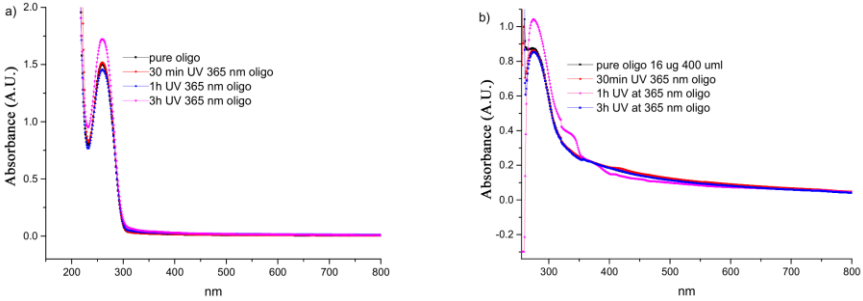

Figure 1.36. UV spectrum of the initial sacrificial oligonucleotide and samples after irradiation in different solvents: (a) DMF:DMSO (1:1) and (b) water.

As shown in **Fig. 1.36**, a change in the absorption maximum occurs only after the third hour of irradiation at a lamp power of 4 W, which necessitates the use of shorter reaction times. In this respect, photoinduced thiol–ene *click* reactions proceed relatively rapidly, and in many cases the reactions are complete within 10 minutes **[27]**. This was confirmed through a series of preliminary experiments involving the *click* reaction of *DHP–AGE₃* with the low-molecular-weight thiol cysteamine and with a thiol-functionalized *PEG* of comparable molar mass to the oligonucleotide. These experiments allowed optimization of the reaction time and conditions for the successful performance of the photoinduced thiol–ene *click* reaction between the thiol-functionalized oligonucleotide (*ThiolC6-oligo*) and *DHP–AGE₃* (**Fig. 1.37**).

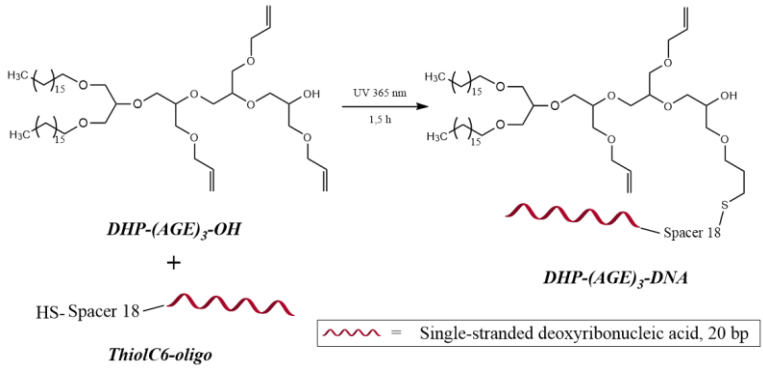

Figure 1.37. Reaction scheme for the synthesis of *DHP-(AGE)₃-DNA* via thiol–ene click

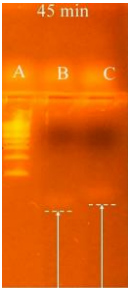

Figure 1.38. Agarose gel electrophoresis of the oligonucleotide before and after conjugation with *DHP*.
(A) Marker
(B) *ThiolC6-oligo*
(C) *DHP-(AGE)₃-DNA*

Successful completion of the reaction was demonstrated by agarose gel electrophoresis (**Fig. 1.38**), which shows a decrease in the electrophoretic mobility of the conjugate in the gel compared to the starting oligonucleotide, as expected considering its higher mass-to-charge ratio.

2.2.2. Conjugation via azide–alkyne *click*

The second method for obtaining a nucleolipid with an analogous architecture was based on the more widely used azide–alkyne *click* reaction. The reaction was carried out between *DHP–EO₇–N₃* and a DBCO-functionalized oligonucleotide (*DBCO–Oligo*) (**Fig. 1.39**). The advantage of this approach is the avoidance of copper salts required in classical Cu (I)-catalyzed azide–alkyne cycloaddition, due to the highly strained cyclooctyne ring in DBCO. The high reactivity of DBCO allows the reaction to proceed almost instantaneously after mixing the two reactants in a wide range of solvents, including bioorthogonal conditions. In the present example, a DMF:DMSO (1:1) mixture was selected as the solvent because of the good solubility of *DHP–EO₇–N₃* in this system and the stability of the oligonucleotide under these conditions.

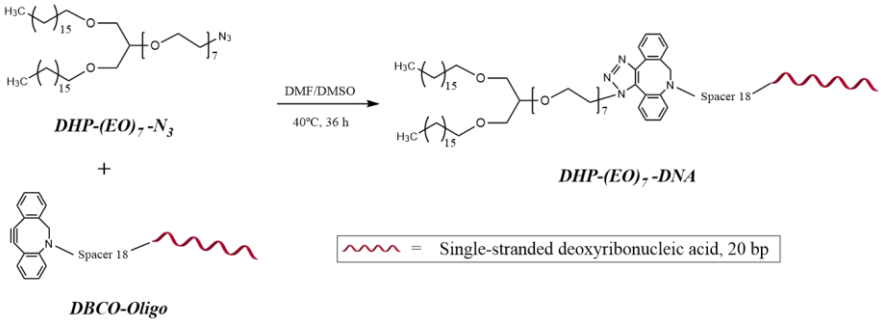

Fig. 1.39. Scheme of the reaction for the preparation of *DHP-(EO)₇–DNA* via azide–alkyne *click*.

Analogously to the previous *click* reaction, successful completion of the reaction was confirmed by agarose gel electrophoresis, which again showed a reduced electrophoretic mobility of the conjugate in the agarose gel (**Fig. 1.40**).

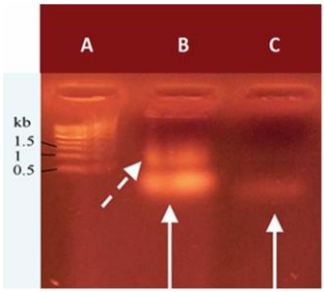

Figure 1.40. Gel electrophoresis of the oligonucleotide before and after conjugation with *DHP.*
(A) Marker
(B) *DHP-(EO)$_7$-DNA* (the dashed arrow indicates a fraction of associated molecules)
(C) *DBCO-Oligo*

The nucleolipids were used for the preparation of liposome-based SNAs through their co-assembly with the phospholipid 1,2-dipalmitoylphosphatidylcholine (*DPPC*) and cholesterol (*Chol*) by the thin-film hydration method. After extrusion, vesicular particles were obtained in which the nucleolipids intercalate into the lipid membrane through their lipid-mimetic fragment (*DHP*), while the oligonucleotide chains orient radially toward the aqueous phase, forming the characteristic *DNA* oligonucleotide shell of SNAs.

For *DHP-(EO)$_7$–DNA*, another type of SNA was also investigated and characterized, formed by spontaneous self-assembly of the nucleolipid in aqueous solution (**Table 7**).

Nanoparticle	R_h (nm)	R_g (nm)	Number of oligonucleotides per particle	ζ (mV)
***DHP-(AGE)$_3$-DNA* (liposomes)**	57.1 ± 2.9	-	3880 ± 194	-911 ± 0.36
***DHP-(EO)$_7$-DNA* (aggregates)**	115.1	112.0 ± 28	88 000	-31.9
***DHP-(EO)$_7$-DNA* (liposomes)**	66.6 ± 0.9	78.0 ± 0.3	3430 ± 92	-17.8 ± 0.5

Table 7. Characteristics of the obtained SNAs based on data from static, dynamic, and electrophoretic light scattering.

Characterization of the obtained SNAs was carried out using a combination of static, dynamic, and electrophoretic light scattering, while their morphology was visualized by Cryo-TEM. Dynamic and static light scattering was used to determine the hydrodynamic and gyration radii of the nanostructures in aqueous solution, whereas electrophoretic light scattering provided information on their ζ-potential (**Fig. 1.41**).

The hydrodynamic radii of the liposomal SNAs were in the range of 55–70 nm, while the vesicular SNAs obtained through self-assembly of *DHP-(EO)$_7$–DNA* exhibited significantly larger sizes, with a hydrodynamic radius of approximately 115 nm (**Table 7**). Both types of structures exhibited ζ-potentials with more negative values compared to control liposomes prepared using the same protocol in the absence of nucleolipids, confirming the exposure of the oligonucleotide corona toward the aqueous phase.

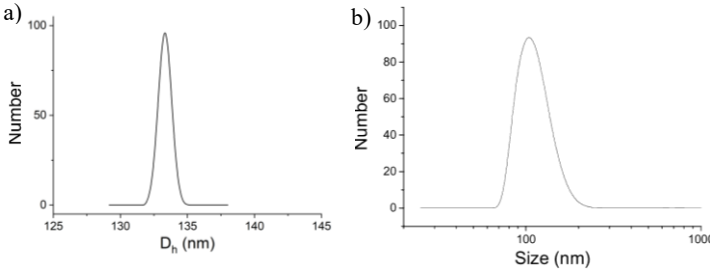

Figure 1.41. Size distribution of liposomal SNAs based on DLS measurements: (a) *DHP-(EO)$_7$-DNA* and (b) *DHP-(AGE)$_3$-DNA*.

The static light scattering data related to the molar mass of the aggregates allowed calculation of the number of nucleolipids per particle. For the self-assembled vesicles, this was determined by directly relating the molar mass of the aggregate to the molar mass of the nucleolipid. For the liposome-based SNAs, the particle surface area was calculated from the *R*g data obtained from DLS, after which N_{agg} was determined assuming that the surface area of one *DPPC*/nucleolipid molecule is 0.65 nm². The number of oligonucleotides was calculated considering that nucleolipids constituted two mol% of the initial mixture used for liposome preparation.

The morphology of the particles was directly visualized by Cryo-TEM, which allowed unequivocal identification of unilamellar vesicular structures and confirmed their liposomal nature (**Fig. 1.42**).

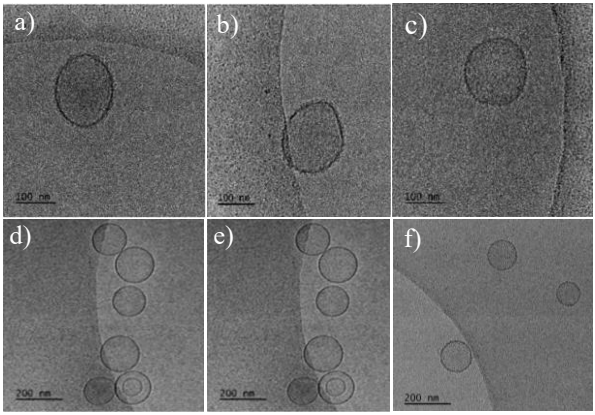

Figure 1.42. Cryo-TEM images: (a–c) vesicles formed by self-assembly of *DHP-(EO)$_7$-DNA*; (d–e) liposomal SNAs obtained by intercalation of DHP-(EO)$_7$-DNA; (f) SNAs obtained by intercalation of *DHP-(AGE)$_3$-DNA*.

The biological properties of the obtained SNAs were evaluated by investigating their cellular internalization, resistance to enzymatic degradation, and colloidal stability in biologically relevant media. Cellular experiments performed with human epithelial cells demonstrated that the liposome-based SNAs are efficiently internalized by the cells without the need for transfection agents, which is a characteristic behavior of SNA architectures. Fluorescence visualization enabled direct monitoring of the distribution of the nanostructures in the cellular environment and confirmed their intracellular internalization (**Fig. 1.43**). A detailed description of the performed studies is presented in **[28,29]**.

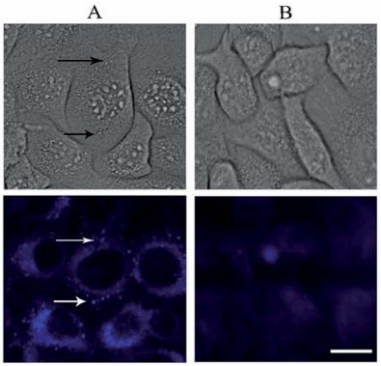

Figure 1.43. Microscopic images of A549 cells: (A) 30 min after treatment with liposomes containing *DHP-(EO)$_7$-DNA*; (B) control cells not treated with SNAs. The scale bar (15 nm) applies to all images. Arrows indicate vesicles internalized within the cells.

The nucleolipids developed in this way, together with the liposomal SNAs obtained from them, represent a new class of functional nanostructures that combine the properties of lipid and nucleic acid systems. This approach opens prospects for the development of a new generation of biocompatible and programmable nanomaterials with applications in nanomedicine and molecular diagnostics.

3. Preparation of linear polystyrenes bearing grafted nucleic acids

As mentioned in Section III.2, spherical nucleic acids represent a highly promising platform with significant potential in gene therapy. In the present work, in addition to nucleolipids used for the preparation of liposomal SNAs, amphiphilic polymer–oligonucleotide conjugates capable of self-assembling in aqueous solution to form SNAs with a polymer core were also developed. The conjugates were obtained by grafting appropriately functionalized nucleotides onto polystyrene copolymers with different topologies (**Fig. 1.44**).

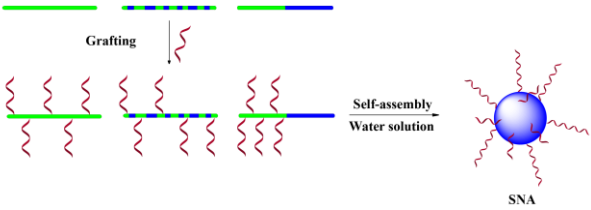

Figure 1.44. General scheme for the preparation of polymers with grafted oligonucleotides and their subsequent self-assembly in aqueous solution into SNAs.

Three polymers based on *styrene* and its derivative, *(4-chloromethyl)styrene*, were synthesized via nitroxide-mediated polymerization. The polymers included a homopolymer of *(4-chloromethyl)styrene*, PCMS; a statistical copolymer of *(4-chloromethyl)styrene* with styrene, *P(S-stat-CMS)*; and a block copolymer of *(4-chloromethyl)styrene* and *styrene*, *PS-block-PCMS*. Subsequently, the polymers were functionalized with azide groups through a substitution reaction with sodium azide, and DBCO-functionalized oligonucleotides (*DBCO–Oligo*) were grafted onto the resulting functionality via azide–alkyne cycloaddition in the absence of a catalyst (**Fig. 1.45**).

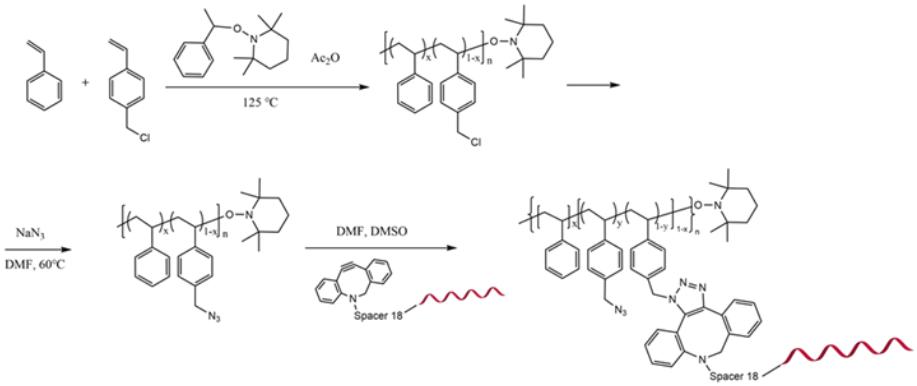

Figure 1.45. Reaction scheme illustrating the grafting of oligonucleotide chains onto the statistical copolymer *P(S-stat-AMS)* via azide–alkyne click reaction.

The polymerizations were carried out at 125 °C in sealed ampoules under vacuum, using 1-phenyl-1-(2,2,6,6-tetramethyl-1-piperidinyloxy)ethane as the initiator in the presence of a catalytic amount of acetic anhydride acting as an activator.

The homopolymer as well as the statistical copolymer were obtained by direct mixing of the monomers, initiator, and catalyst followed by polymerization for several hours, whereas the block copolymer was synthesized through initial homopolymerization of styrene, isolation of the product, and its subsequent use as a macroinitiator for the polymerization of (4-chloromethyl)styrene.

Polymer	**M_w (GPC) g/mol**	***Đ*** **(GPC)**	**wt% (PCMS)**	**wt% (PS)**
PCMS	11 000	1.45	100 (72 monomer units)	0 (0 monomer units)
P(S-stat-CMS)	10 000	1.28	30 (20 monomer units)	70 (68 monomer units)
PS-block-PCMS	16 500	1.14	11 (12 monomer units)	89 (142 monomer units)

Table 8. Molar mass characteristics of the obtained polystyrenes.

In this way, three polymers containing chlorine atoms in their side chains were obtained (**Table 8**). In a subsequent reaction, these chlorine atoms were substituted with azide groups through a nucleophilic substitution reaction with sodium azide. The ^{1}H NMR spectra of the chloro- and azide-functionalized polymers are shown in **Fig. 1.46**. Quantitative substitution of the chlorine atoms is confirmed by the shift of the signal at 4.5 ppm, corresponding to the benzylic methylene group bonded to a chlorine atom, to 4.2 ppm, characteristic of a benzylic methylene group bonded to an azide functionality.

The performed functionalization enabled the grafting of oligonucleotide chains onto the polystyrene polymers. For this purpose, DBCO-functionalized oligonucleotides with a nonspecific base sequence were used. In order to achieve precise control over the grafting density and to reduce steric hindrance between individual oligonucleotide chains, approximately one oligonucleotide was grafted per 2000 g/mol of polymer, corresponding to five grafted oligonucleotide chains for *PAMS* and *P(S-stat-AMS)*, and seven grafted oligonucleotides for *PS-block-PAMS*. Due to the polyfunctionality of the polystyrene chains, the azide groups were present in excess relative to the triple bonds of the oligonucleotides. This ensured practically quantitative conjugation of the oligonucleotide chains onto the polymer backbone, while the average grafting degree and the yields were calculated by UV spectrophotometry.

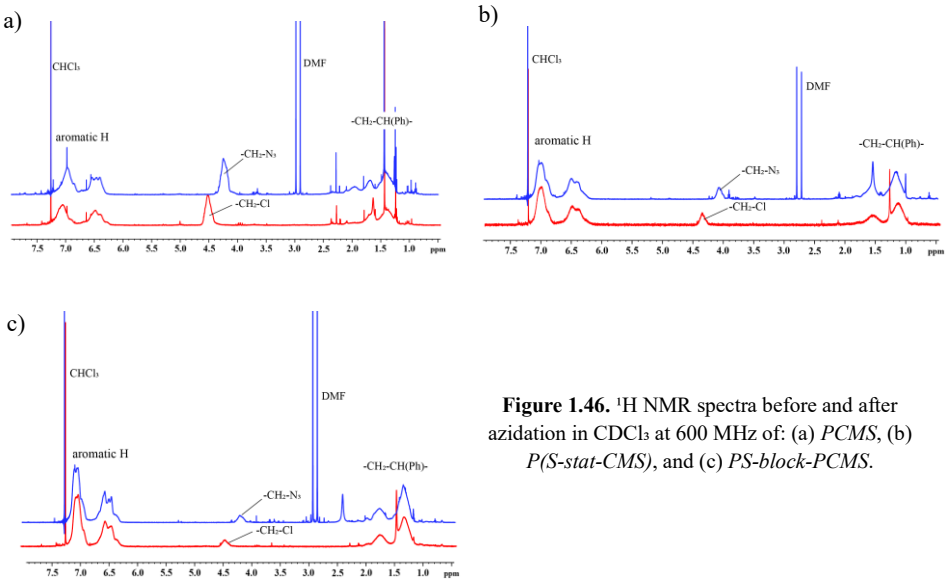

Figure 1.46. ^{1}H NMR spectra before and after azidation in $CDCl_3$ at 600 MHz of: (a) *PCMS*, (b) *P(S-stat-CMS)*, and (c) *PS-block-PCMS*.

Figure 1.47. Photographs from the dialysis of the conjugates. The solutions are transparent and no precipitation is observed.

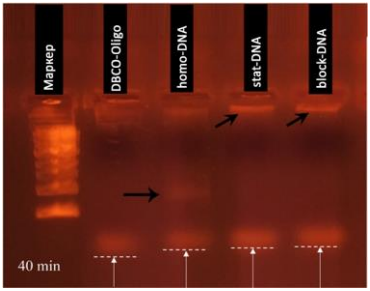

Figure 1.48. Agarose gel electrophoresis of the obtained conjugates.
DBCO-Oligo – starting oligonucleotide.
homo-DNA – *P((AMS-graft-Oligo)-stat-AMS)*
stat-DNA – *P(S-stat-(AMS-graft-Oligo)-stat-AMS)*
block-DNA – *PS-b-P((AMS-graft-Oligo)-stat-AMS)*

The obtained conjugates were completely water-soluble (**Fig. 1.47**), in contrast to the starting polystyrenes, and their molar mass was significantly higher than that of the starting materials, which was confirmed by the greater retardation of their migration during agarose gel electrophoresis (**Fig. 1.48**). Further evidence for the successful reaction was provided by the fact that purification was performed by dialysis through a 15 kDa MWCO cellulose membrane, through which both the starting polystyrenes and the oligonucleotides would normally pass. In all three cases, the products remained inside the dialysis tubing with nearly quantitative yields.

In aqueous solution, the conjugates exhibit a tendency toward self-association, forming particles composed of a dense polymer core surrounded by a corona of radially oriented oligonucleotide chains, which classifies them as SNAs. Characterization of the obtained aggregates was carried out using a combination of static, dynamic, and electrophoretic light scattering (**Table 9**). Their diameters are in the range of 80–100 nm, while the aggregation number varies between 350 and 600 for the different conjugates. As expected considering the morphological characteristics of SNAs, all three types of particles exhibit a negative ζ-potential in the range of −16 to −18 mV. The morphology of the particles was confirmed by TEM, which revealed spherical particles with sizes consistent with the values obtained from light scattering (**Fig. 1.49**).

SNA	R_g (nm)	R_h (nm)	R_g/R_h	N_{agg}	M_w (g/mol)	ζ (mV)
P((AMS-graft-Oligo)-stat-AMS)	40.6	45.5	0.89	367	16.8 x 10^6	-17.9
P(S-stat-(AMS-graft-Oligo)-stat-AMS)	41.1	48.1	0.85	577	25.8 x 10^6	-16.8
PS-b-P((AMS-graft-Oligo)-stat-AMS)	51.2	49.7	1.03	524	37.8 x 10^6	-15.6

Table 9. Characteristics of the obtained SNAs determined by dynamic, static, and electrophoretic light scattering.

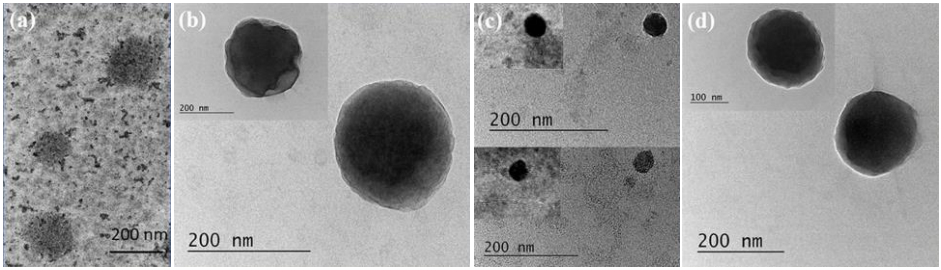

Figure 1.49. TEM images of polymer–oligonucleotide conjugates in aqueous solution: (a, b) *P((AMS-graft-Oligo)-stat-AMS)*; (c) *P(S-stat-(AMS-graft-Oligo)-stat-AMS)*; (d) *PS-b-P((AMS-graft-Oligo)-stat-AMS)*.

The biological properties of the obtained SNAs were tested on A549 cell lines. At all tested concentrations, the particles did not exhibit cytotoxic effects. For all three types of SNAs, an increase in the basal metabolic activity of the cells was observed, indicating the presence of a cellular response to the introduced structures. Efficient penetration through the plasma membrane was observed 30 minutes after treatment of the cells with the SNAs, in the absence of a cationic transfection agent. In addition, two of the three types of SNAs demonstrated significantly increased resistance to enzymatic degradation by DNase (**Fig. 1.50** and **Fig. 1.51**). A detailed description of the results of these studies is provided in **[30]**.

The obtained results demonstrate a new approach for the construction of three-dimensional nanostructures carrying nucleic acids through the self-assembly of polymer–oligonucleotide conjugates. The established relationships between molecular architecture, oligonucleotide chain density, and the properties of the resulting aggregates provide a basis for the design of new SNA-like systems with potential biomedical applications.

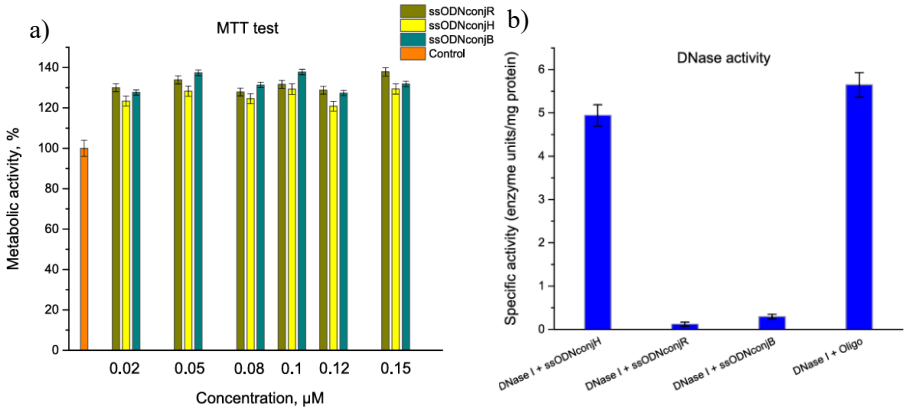

Figure 1.51. (a) Metabolic activity of A549 cells 6 h after incubation with SNAs. The values are compared with untreated control cells (Control).
(b) Specific enzymatic activity of DNase toward the three aggregates. DNase + Oligo represents the control experiment using the initial DBCO-Oligo.
ssODNconjH – *P((AMS-graft-Oligo)-stat-AMS)*
ssODNconjR – *P(S-stat-(AMS-graft-Oligo)-stat-AMS)*
ssODNconjB – *PS-b-P((AMS-graft-Oligo)-stat-AMS)*

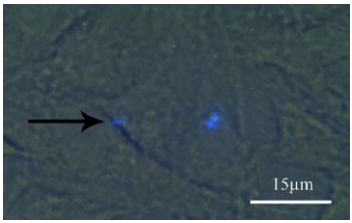

Figure 1.50. A549 cells observed under fluorescence microscopy 30 min after treatment with *P((AMS-graft-Oligo)-stat-AMS)*. Internalized particles are indicated by arrows.

4. Preparation of linear and star-shaped copolymers of polyglycidol (*PG*) and *poly(ε-caprolactone) (PCL)*

As noted in the introduction of the present work, one of the most important biomedical applications of polymers is related to the development of nanocarriers for drug delivery. Several pharmaceutical formulations are already available on the market in which the active compound is encapsulated within a hydrophobic micellar core, while a significant number of others are currently in the final stages of clinical trials.

An important requirement in the design of micellar nanocarriers is that the polymer materials from which they are constructed must be biocompatible and/or biodegradable. At present, the main polymers that

have reached the market and fulfill this role are *PEG* and *PLA*. Nevertheless, a large number of other polymers demonstrate similar or even superior properties for solubilizing hydrophobic substances, accompanied by reduced toxicity, lower immunogenicity, and improved stability.

One of the polymers whose properties have been widely investigated as an alternative to *PEG* is *PG*. A polymer similar to *PLA* in terms of properties, chemical nature, and method of preparation is *PCL*, which, like *PLA*, is a biodegradable polyester. In order to investigate the potential of these two polymers for the preparation of micellar nanocarriers, a series of their copolymers with different topologies, compositions, and molar masses were synthesized. The syntheses were based on a convergent-type strategy, in which the two blocks are prepared and functionalized separately and only subsequently coupled, due to the instability of *PCL* under the conditions of anionic polymerization.

4.1. Preparation of alkyne-functionalized *poly(ethoxyethyl glycidyl ether)s* (*PEEGE*)

For the synthesis of the polyglycidol block of the copolymers, "living" anionic polymerization of its protected analogue, *ethoxyethyl glycidyl ether*, was employed. Two polymers with molar masses of 3000 and 8000 g/mol were obtained. For the synthesis of the lower-molar-mass polymer, the potassium salt of cyclohexanol was used as the initiator, and the reaction was carried out in bulk. Potassium *tert*-butoxide was used as the catalyst for the preparation of the higher-molar-mass polymer, and the polymerization was conducted in DMSO as the solvent. In both cases, after consumption of the monomer, a short *PPO* spacer was introduced at the end of the polymer chain by adding propylene oxide prior to termination of the polymerization. General synthetic schemes of the performed reactions are presented in **Fig. 1.52**. The obtained polymers were characterized by GPC (**Fig. 1.53**), FTIR, and ^{1}H NMR spectroscopy. The degree of polymerization (**Table 10**) was determined by ^{1}H NMR after deprotection of a small portion of the polymers (**Fig. 1.54**).

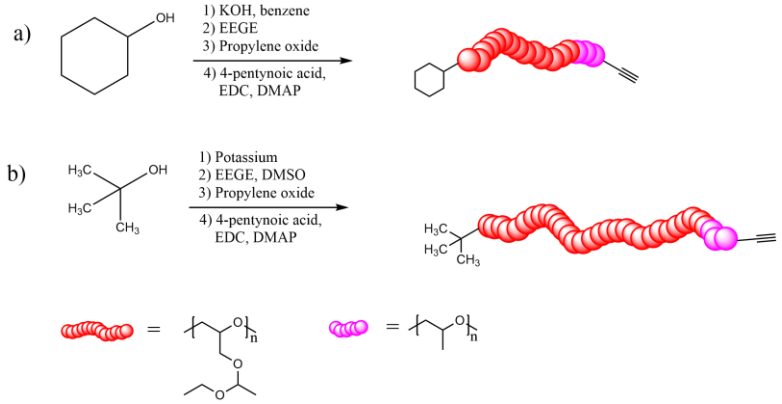

Figure 1.52. Schematic representation of the synthesis and functionalization of alkyne-terminated *PEEGE*.

Subsequently, the two polymers were functionalized by esterification with *4-pentynoic acid* in order to introduce a terminal alkyne at the end of the polymer chain. The reaction was carried out in chloroform using the EDC/DMAP system as the condensation agent. In this case as well, the presence of the *PPO* spacer plays a key role, since in its absence the aforementioned esterification does not proceed quantitatively **[4]**. The obtained polymers possessed fully esterified terminal groups, as determined from the integral ratio of the signals at 2.5 and 2.3 ppm, corresponding to the protons of *4-pentynoic acid*, and those at 4.65 ppm corresponding to the methine protons of *PEEGE* in the ^{1}H NMR spectrum (see **1.2.1**).

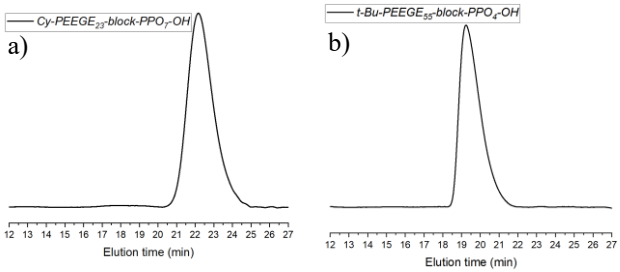

Figure 1.53. Gel permeation chromatograms of *Cy-PEEGE$_{23}$-block-PPO$_7$-OH* (a) *and t-Bu-PEEGE$_{55}$-block-PPO$_4$-OH* (b).

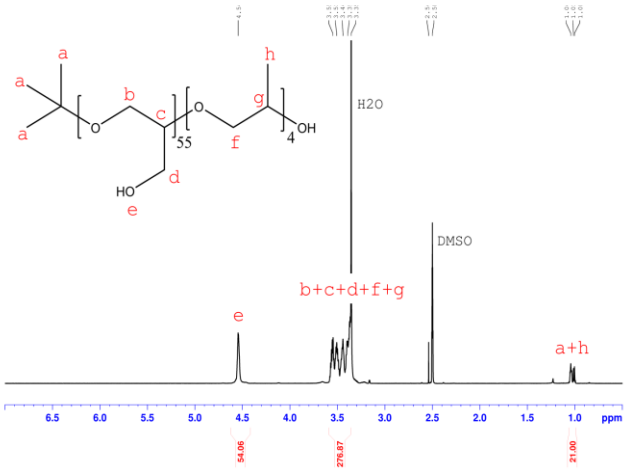

Figure 1.54. ^{1}H NMR spectrum of *t-Bu-PG$_{55}$-b-PPO$_4$-OH*. After deprotection, the degree of polymerization was determined from the integral ratio of the signals corresponding to the methyl protons (1.01 ppm) to those of the remaining protons of the polymer backbone.

Polymer	Degree of polymerization of *PEEGE* (NMR)	$M_{n(NMR)}$ (g/mol)	$M_{n(GPC)}$ (g/mol)	$M_{w(GPC)}$ (g/mol)	*Đ*
Cy-PEEGE$_{23}$-block-PPO$_7$-OH	23	4880	2670	2980	1.12
t-Bu-PEEGE$_{55}$-block-PPO$_4$-OH	55	8430	6470	7750	1.20

Table 10. Molecular mass characteristics of *Cy-PEEGE$_{23}$-block-PPO$_7$-OH* and *t-Bu-PEEGE$_{55}$-block-PPO$_4$-OH*.

4.2. Preparation of linear and star-shaped azide-terminated *poly(ε-caprolactone)s*

For the construction of the hydrophobic block of the copolymers, azide-terminated *PCL* with linear and star-shaped architecture were prepared. In view of the subsequent studies related to the behavior of the copolymers in aqueous solution, it was necessary for the *PCL* used to possess identical molar mass (2000

g/mol). Hydroxyl-terminated bi- (*HO-PCL$_{16}$-OH*), tri- (*3-star-PCL$_6$-OH*), and tetrafunctional polymers (*4-star-PCL$_4$-OH*) were used. The first two are commercially available products (CAPA2225 and CAPA3201, respectively), while *4-star-PCL4-OH* was obtained by chain extension of *4-star-PCL$_2$-OH* (CAPA4101). The polymerization was carried out in bulk in the presence of tin(II) octoate. GPC analysis showed a clear decrease in the elution time, demonstrating an increase in the hydrodynamic size of the polymer and consequently its molar mass. The degree of polymerization was calculated by ^{1}H NMR spectroscopy from the integral ratio between the methylene groups of the initiator (4.10 ppm) and those corresponding to the protons of the monomer units (**Table 11**, **Fig. 1.57** below).

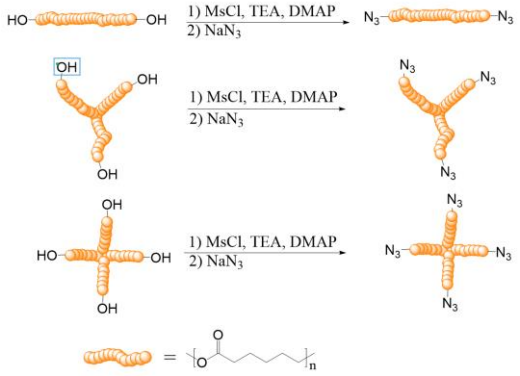

Figure 1.55. Schematic representation of the azide functionalization of linear and star-shaped – OH-terminated *PCL*.

The conversion of the terminal hydroxyl groups of *PCL* into azide groups was performed in two steps, consisting of their activation through esterification with mesyl chloride followed by substitution of the mesylate groups via reaction with sodium azide. A general scheme of the described transformations is presented in **Fig. 1.55**. Complete characterization of the intermediate and final products was carried out by FTIR and ^{1}H NMR spectroscopy (**Fig. 1.56**, **1.57**).

Polymer	Degree of polymerization (NMR)	$M_{n(NMR)}$ (g/mol)	$M_{n(GPC)}$ (g/mol)	$M_{w(GPC)}$ (g/mol)	Đ
N$_3$-PCL$_{16}$-N$_3$	16	1980	3380	4370	1.29
3-star-PCL$_6$-N$_3$	18	2260	1760	1950	1.11
4-star-PCL$_4$-N$_3$	16	2060	1730	1870	1.08

Table 11. Molecular mass characteristics of linear and star-shaped azide-functionalized *PCL*.

4.3. Preparation of *PCL–PG* block copolymers with different architectures

The preparation of *PCL–PEEGE* block copolymers with different architectures was carried out via copper-catalyzed azide–alkyne *click* reaction between the terminal alkyne of *PEEGE* and the azide groups at the ends of *PCL*. The reactions were catalyzed by copper(I) bromide coordinated with PMDETA (**Fig. 1.58**). After completion of the reaction time, the catalyst was removed by column chromatography using neutral alumina as the stationary phase and THF as the eluent. Additional purification from unreacted polymer chains was performed by dialysis in a methanol:water mixture (9:1). The products were characterized by GPC and

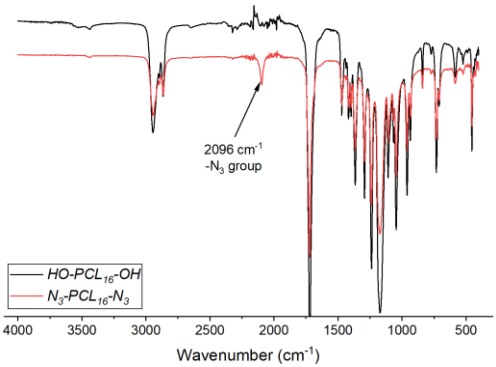

Figure 1.56. IR spectra of *HO-PCL₁₆-OH* and *N₃-PCL₁₆-N₃*.

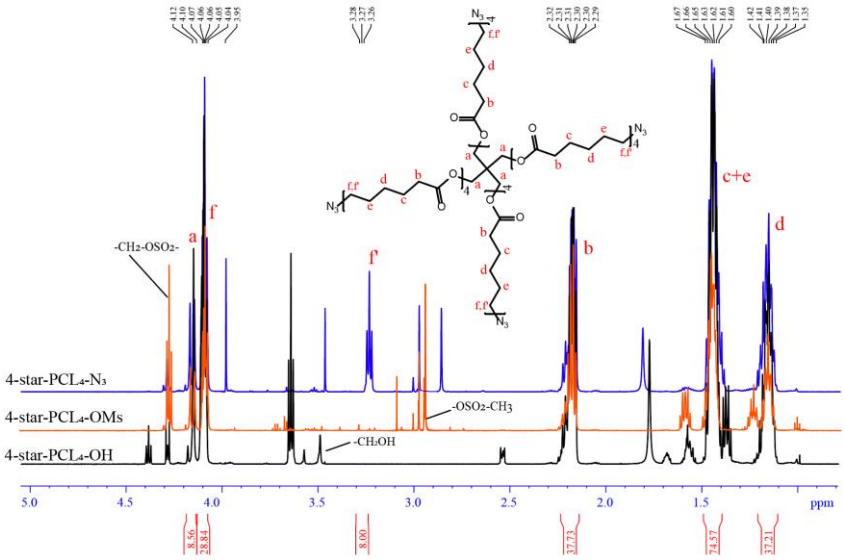

Figure 1.57. ^{1}H NMR spectra of *4-star-PCL₄-N₃* and its precursors *4-star-PCL₄-OH* and *4-star-PCL₄-OMs* in $CDCl_3$ at 600 MHz. The indicated integral ratios correspond to *4-star-PCL₄-N₃*.

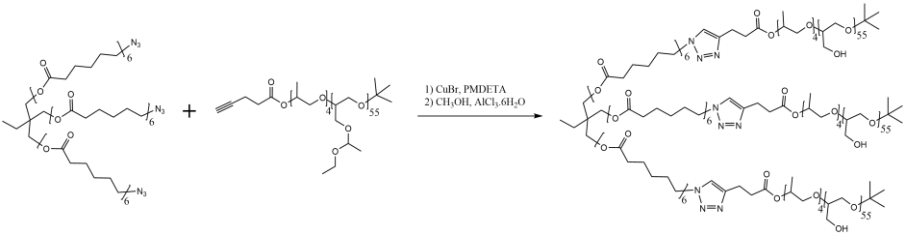

Figure 1.58. Reaction scheme for the synthesis of *3-star-(PCL₆-block-PPO₇-block-PG₅₅-t-Bu)*.

^{1}H NMR spectroscopy. Evidence for the successful reactions was the significant decrease in the elution time in GPC (**Fig. 1.59**), as well as the appearance of a signal at 7.6 ppm in the proton spectrum corresponding to the triazole ring (**Fig. 1.60, 1.61**).

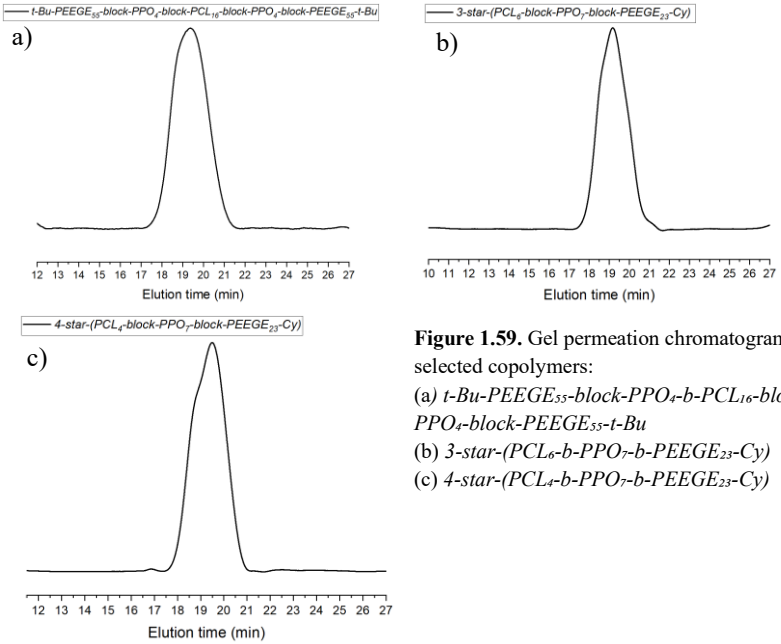

Figure 1.59. Gel permeation chromatograms of selected copolymers:
(a) *t-Bu-PEEGE$_{55}$-block-PPO$_4$-b-PCL$_{16}$-block-PPO$_4$-block-PEEGE$_{55}$-t-Bu*
(b) *3-star-(PCL$_6$-b-PPO$_7$-b-PEEGE$_{23}$-Cy)*
(c) *4-star-(PCL$_4$-b-PPO$_7$-b-PEEGE$_{23}$-Cy)*

In the final stage of the synthesis, the protecting ethoxyethyl groups of the glycidol units in the polymers were removed through reaction with methanol in the presence of a catalytic amount of $AlCl_3.6H_2O$ (see **1.3.1**). Complete deprotection was indicated by the strong decrease in the integral ratio of the signals in the region 1.10–1.30 ppm in the ^{1}H NMR spectrum, corresponding to the methyl protons of the ethoxyethyl group (**Fig. 1.68**). The molar mass characteristics and architecture of the obtained copolymers are summarized in **Table 13**.

Considering the hydrophilic character of *PG* and the hydrophobic nature of *PCL*, the obtained block copolymers exhibit pronounced amphiphilic properties. In combination with the good biocompatibility of the polymer blocks forming them, the products provide opportunities for application in the development of nanocarriers for drugs and biologically active compounds. The different architectures and hydrophilic/hydrophobic block ratios of the copolymers allow detailed investigation of the behavior of this class of materials depending on their composition and topology. One of the already explored applications of some of these polymers is their ability to modify niosomal membranes **[31]**.

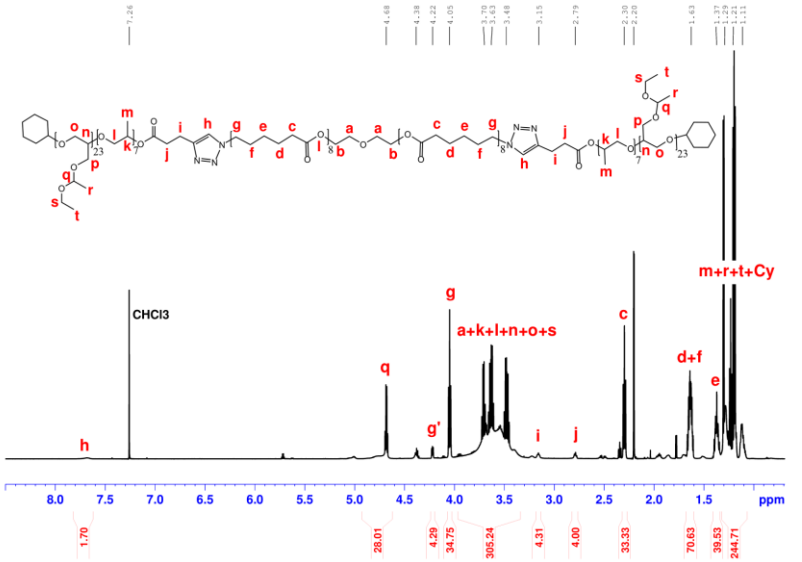

Figure 1.60. ^{1}H NMR spectrum of *Cy-PEEGE$_{23}$-block-PPO$_{7}$-block-PCL$_{16}$-block-PPO$_{7}$-b-PEEGE$_{23}$-Cy* in $CDCl_3$ at 600 MHz.

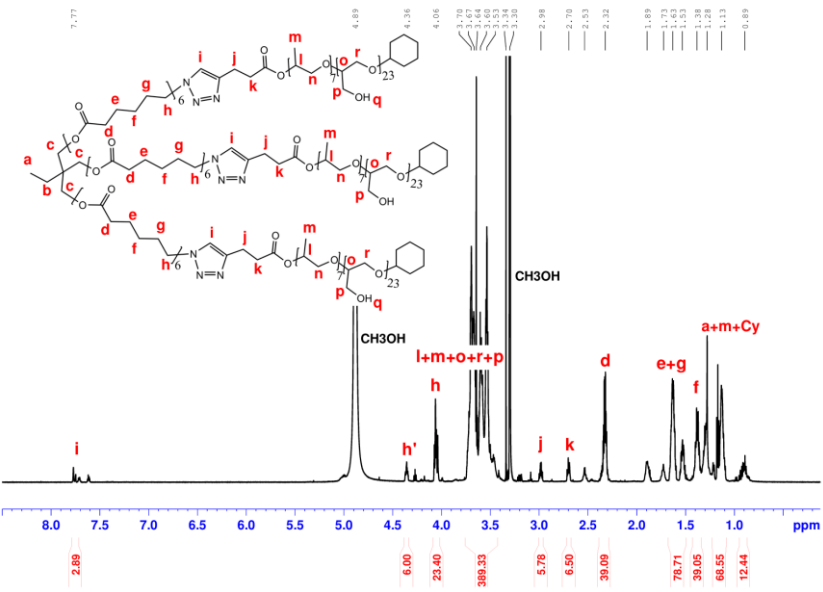

Figure 1.61. ^{1}H NMR spectrum of *3-star-(PCL$_{6}$-block-PPO$_{7}$-block-PG$_{23}$-Cy)* in $CDCl_3$ at 600 MHz.

№	Polymer	$M_{n(NMR)}$	f_A/f_B	Topology
1	***Cy-PG$_{23}$-block-PPO$_7$-block-PCL$_{16}$-block-PPO$_7$-block- PG$_{23}$-Cy***	6 160	1.21	
2	***t-Bu-PG$_{55}$-block-PPO$_4$-block-PCL$_{16}$-block-PPO$_4$-block-PG$_{55}$-t-Bu***	10 560	3.30	
3	***3-star-(PCL$_6$-block-PPO$_7$-block-PG$_{23}$-Cy)***	8 240	1.59	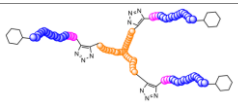
4	***3-star-(PCL$_6$-block-PPO$_4$-block-PG$_{55}$-t-Bu)***	14 910	4.53	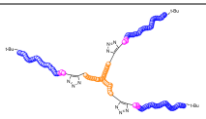
5	***4-star-(PCL$_4$-block-PPO$_7$-block-PG$_{23}$-Cy)***	10 320	1.88	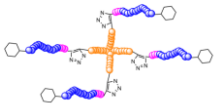
6	***4-star-(PCL$_4$-block-PPO$_4$-block-PG$_{55}$-t-Bu)***	19 140	5.56	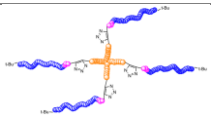

Table 12. Molar mass characteristics and architecture of the obtained copolymers. $M_{n\,(NMR)}$ – number-average molar mass determined by ^{1}H NMR; fA/fB – ratio of the hydrophilic to the hydrophobic mass fraction of the polymers.

Niosomes are vesicular nanostructures with a bilayer membrane composed of non-ionic surfactants, usually in combination with cholesterol. They can encapsulate both hydrophilic and lipophilic substances and are widely used as carriers for the controlled delivery of drugs, genes, and biologically active molecules. For the modification of niosomal membranes, the three copolymers containing shorter *polyglycidol* blocks (numbers **1**, **3**, and **5** in **Table 12**) were selected due to their lower tendency toward self-association under the conditions of niosome formation, as well as their more efficient intercalation into the niosomal membranes. The niosomes were prepared by the thin-film hydration method using a film formed from the surfactants and the respective polymer.

The obtained polymer-modified niosomes exhibit a larger hydrodynamic radius compared with the control, unmodified systems. This effect can be explained by the rigid structure of *PCL* and the resulting increase in membrane curvature, which leads to a larger particle diameter. The integrity of the membrane as well as the vesicular morphology of the niosomes were confirmed by Cryo-TEM (**Fig. 1.62**). The observed particles are predominantly unilamellar, although a small fraction of bilamellar vesicles was also detected. No open pores or structural defects in the membranes were observed, which is an important requirement for the use of these particles in controlled drug delivery.

The loading capacity and release profiles of hydrophobic substances from the niosomes were investigated using cannabidiol (*CBD*) as a model compound **[32]**. The release profiles from niosomes modified with polymer **3** (**Table 13**) are presented in **Fig. 1.63**. A clearly slower release of *CBD* was observed for the

modified niosomes, demonstrating the possibility of tuning the pharmacokinetic profile of such systems by incorporating the synthesized copolymers into the membrane.

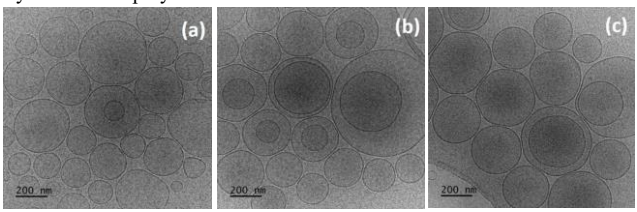

Figure 1.62. Cryo-TEM images of (a) unmodified niosomes, (b) niosomes modified with *3-star-(PCL$_6$-block-PPO$_7$-block-PG$_{23}$-Cy)*, and (c) niosomes modified with *4-star-(PCL$_4$-block-PPO$_7$-block-PG$_{23}$-Cy)*.

The stability of the obtained vesicular systems was monitored over a period of one month by tracking changes in particle size, polydispersity, and ζ-potential (**Table 13**). In comparison with the control group, the modified niosomes exhibited higher colloidal stability, which can be attributed to the copolymers incorporated into the membrane.

Sample	Time	D_h (nm)	PDI	ζ (mV)
Control (unmodified niosomes)	0 h	150±1.1	0.35±0.07	−10.3±1.6
	After 1 month	132±2.8	0.41±0.09	−10.6±2.1
Niosomes, modified with *3-star-(PCL$_6$-blcok-PPO$_7$-block-PG$_{23}$-Cy)*	0 h	235±5.6	0.36±0.02	−11.1±1.7
	After 1 month	228±2.2	0.39±0.05	−11.8±1.2

Table 13. Stability of unmodified niosomes and niosomes modified with polymer **3** (*3-star-(PCL$_6$-block-PPO$_7$-block-PG$_{23}$-Cy)*) after 1 month.

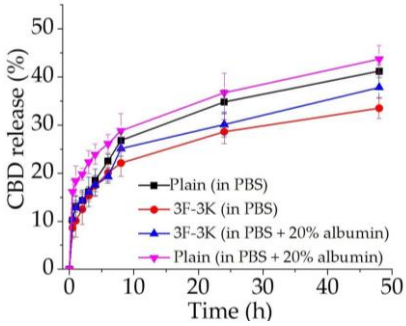

Figure 1.63. Release profiles of CBD from unmodified niosomes and from niosomes modified with polymer **3** (*3-star-(PCL$_6$-b-PPO$_7$-b-PG$_{23}$-Cy)*) under different conditions.

The obtained results clearly demonstrate that amphiphilic PCL–PG block copolymers enable the targeted tuning of key parameters of nanostructured systems—size, colloidal stability, and the release profile of encapsulated hydrophobic compounds. The combination of structural stability, preserved membrane integrity, and tunable pharmacokinetics positions polymer-modified niosomes as a promising platform for the development of intelligent nanocarriers with adjustable properties, suitable for applications in targeted delivery, controlled release, and personalized therapeutic systems.

CONCLUSIONS

Based on the obtained results, the following conclusions can be drawn:

1. A novel synthetic strategy for the preparation of polymer–lipid conjugates has been developed, based on the synthesis of alkyne-/azide-monofunctionalized linear polymers and an alkyne-/azide-functionalized lipid analogue (*DHP*), followed by their conjugation via azide–alkyne click chemistry. **This approach expands the applicability of click reactions and enables the preparation of well-defined hybrid amphiphilic systems suitable for the surface modification of biological membranes.**

2. Two reliable synthetic approaches have been established for the preparation of a new class of nucleolipids, based on highly efficient click reactions for the covalent conjugation of oligonucleotide fragments with lipid analogues. The resulting amphiphilic molecules represent an **effective platform for the construction of spherical nucleic acids (SNAs)**, both via self-assembly and in combination with phospholipids, thereby expanding the possibilities for generating novel SNA architectures.

3. The obtained amphiphilic molecules **demonstrated significant potential as an effective platform for the construction of SNAs**, both through self-assembly and in combination with phospholipids, further broadening the scope for the development of new types of SNAs.

4. A synthetic strategy has been developed for the preparation of polystyrene-based polymers bearing covalently grafted oligonucleotide chains, based on controlled polymerization techniques followed by highly efficient post-polymerization functionalization via click chemistry. The resulting hybrid polymer–oligonucleotide conjugates **enable the formation of polymer-core SNAs, characterized by well-defined structure and tunable architecture**, which underpins their potential for applications in gene transfection and biomedical nanotechnology.

5. Linear and star-shaped polyglycidol–poly(ε-caprolactone) copolymers with varying composition, molecular weight, and topology have been successfully synthesized through the combination of controlled polymerization techniques and click chemistry. These systems exhibit a high degree of structural diversity and **represent promising platforms for the development of nanocarriers for the delivery of biologically active compounds and drug molecules**. The developed synthetic strategy enables the targeted preparation of *PG–PCL* block copolymers with diverse architectures and controllable properties.

CONTRIBUTIONS OF THE DISSERTATION

1. **Original synthetic strategies have been developed** for the preparation of biocompatible and/or biodegradable macromolecules through the combination of anionic, cationic, and controlled radical polymerization techniques, enabling precise control over molecular weight, polymer architecture, and functionality.

2. **A novel phospholipid-mimicking secondary alcohol (DHP) has been synthesized**, and efficient approaches for its functionalization and subsequent conjugation with polymers and nucleic acids have been developed.

3. **Efficient conjugation methods based on click reactions** (azide–alkyne and thiol–ene), conducted under catalyst-free conditions, have been developed and applied for the preparation of polymer–nucleic acid and lipid–nucleic acid conjugates.

4. **A new class of nucleolipids and polymer–oligonucleotide conjugates has been obtained**, capable of forming supramolecular structures of the spherical nucleic acid (SNA) type with diverse architectures (liposomal and polymeric cores).

5. **Amphiphilic block copolymers** (*PG–PCL* with linear and star-shaped architectures) with controllable composition, molecular weight, and topology **have been successfully synthesized.**

6. **A correlation between molecular architecture and physicochemical properties** (self-assembly, stability, morphology) of the obtained systems **has been established**, enabling the targeted tuning of their characteristics.

7. **The possibility for fine-tuning functional properties** (including release profiles and colloidal stability) through molecular design and structural modification **has been demonstrated.**

8. **The potential of the developed systems** for application as nanocarriers for the delivery of nucleic acids, chemotherapeutics, and biologically active compounds **has been demonstrated.**

LIST OF PUBLICATIONS, CITATIONS AND SCIENTIFIC COMMUNICATIONS PRESENTING THE RESULTS OF THE DISSERTATION

PUBLICATIONS

1. Dimitrov, E.; Toncheva-Moncheva, N.; Bakardzhiev, P.; Forys, A.; Doumanov, J.; Mladenova, K.; Petrova, S.; Trzebicka, B.; Rangelov, S. *Nucleic Acid-Based Supramolecular Structures: Vesicular Spherical Nucleic Acids from a Non-Phospholipid Nucleolipid*. **Nanoscale Advances** 2022, *4*, 3793–3803, JIF 4.7, Q1, DOI: 10.1039/d2na00527a
2. Dimitrov, E.; Toncheva-Moncheva, N.; Bakardzhiev, P.; Forys, A.; Doumanov, J.; Mladenova, K.; Petrova, S.; Trzebicka, B.; Rangelov, S. *Original Synthesis of a Nucleolipid for Preparation of Vesicular Spherical Nucleic Acids*. **Nanomaterials** 2022, *12*, 3645, JIF 5.3, Q1, https://doi.org/10.3390/nano12203645
3. Dimitrov, E.; Toncheva-Moncheva, N.; Doumanov, J. A.; Mladenova, K.; Petrova, S.; Pispas, S.; Rangelov, S. *Three-Dimensional Nucleic Acid Nanostructures Based on Self-Assembled Polymer–Oligonucleotide Conjugates of Comblike and Coil-Comb Chain Architectures*. **Biomacromolecules** 2023, *24* (5), 2213–2224. JIF 5.5, Q1, https://doi.org/10.1021/acs.biomac.3c00126
4. Gugleva, V.; Ahchiyska, K.; Georgieva, D.; Mihaylova, R.; Konstantinov, S.; Dimitrov, E.; Toncheva-Moncheva, N.; Rangelov, S.; Forys, A.; Trzebicka, B.; Momekova, D. *Development, Characterization and Pharmacological Evaluation of Cannabidiol-Loaded Long Circulating Niosomes*. **Pharmaceutics** 2023, *15*, 2414, JIF 4.9, Q1, https://doi.org/10.3390/pharmaceutics15102414
5. Dimitrov, E.; Aleksandrov, K.; Toncheva-Moncheva, N.; Shestakova, P.; Forys, A.; Trzebicka, B.; Rangelov, S. *Self-Assembly and Structural Polymorphism of Polymer–Lipid Mimetics Prepared by Azide–Alkyne Cycloaddition*. **Macromolecules** 2026, ASAP, JIF 5.2, Q1, https://doi.org/10.1021/acs.macromol.5c02775

SCIENTIFIC COMMUNICATIONS

1. XVI Scientific Session “Young Scientists in the World of Polymers”, Sofia Tech Park, Sofia, 04.03.2025
   Water-Soluble Polyglycidol-Grafted Ladder Calix Resorcinarene Oligomers with Open Chain and Cyclic Topologies: Synthesis and Characterization, **poster**
   Erik Dimitrov, Hristo Penchev, Christo Novakov, Emi Haladjova, Sibela Doleva, Stanislav Rangelov
2. International Scientific Conference “Silesian Meetings on Polymer Materials” POLYMAT 2025, Zabrze, Poland, 29.05.2025
   Design and synthesis of novel polymer–lipid conjugates with potential applications in drug delivery
   Erik Dimitrov, Krum Alexandrov, Natalia Toncheva-Moncheva, Pavletta Shestakova, Stanislav Rangelov
3. XV Scientific Session “Young Scientists in the World of Polymers”, Institute of Polymers – BAS, Sofia, 06.06.2024
   Синтез на съполимери на поли(2-изопропил-2-оксазолин) и полиетиленимин с потенциални приложения за генна терапия, **oral presentation, award for best presentation**
   Ерик Димитров, Сибела Долева, Наталия Тончева-Мончева, Станислав Рангелов

4. Annual Scientific Session Dedicated to the 155th Anniversary of the Bulgarian Academy of Sciences, Institute of Organic Chemistry with Centre of Phytochemistry, Sofia, 24–25.04.2024
Preparation of polymer amphiphiles for surface modification of niosomes, **poster, award for best poster**
Erik Dimitrov, Krum Alexandrov, Natalia Toncheva-Moncheva, Pavleta Shestakova, Denitsa Momekova, Stanislav Rangelov
5. XXI Poster Session for Young Scientists, PhD Students and Students at UCTM in the Section "Chemical Technologies", UCTM, Sofia, 20.07.2024
Synthesis of Amphiphilic Polymers for Surface Modification of Niosomes, **poster**
Erik Dimitrov, Krum Alexandrov, Natalia Toncheva-Moncheva, Pavleta Shestakova, Denitsa Momekova, Stanislav Rangelov
6. XIII Scientific Session "Young Scientists in the World of Polymers", Institute of Polymers – BAS, Sofia, 02.07.2022
Synthesis of polymer nonphospholipid conjugates for surface modification of niosomes, **oral presentation, award for best presentation**
Erik Dimitrov, Natalia Toncheva-Moncheva, Pavel Bakardzhiev, Rumena Stancheva, Denitsa Momekova, Aleksander Forys, Barbara Trzebicka, Stanislav Rangelov
Non-phospholipid conjugate of poly(2-isopropyl-2-oxazoline) for design of surfactant vesicles, **poster**
Enis Hasan, Erik Dimitrov, Natalia Toncheva-Moncheva, Stanislav Rangelov
7. International Scientific Conference "Silesian Meetings on Polymer Materials" POLYMAT 2022, Zabrze, Poland, 17.03.2022
Nucleolipid Vesicles: Supramolecular Structures Resembling Spherical Nucleic Acids, **poster, award for best poster**
Erik Dimitrov, Natalia Toncheva-Moncheva, Pavel Bakardzhiev, Aleksander Forys, Jordan Doumanov, Kirilka Mladenova, Svetla Petrova, Barbara Trzebicka, Stanislav Rangelov
Novel amphiphilic polyglycidol/poly(ε-caprolactone) and polyglycidol/poly(α-cinnamyl-ε-caprolactone) copolymers as highly effective nanocarriers, **poster**
Natalia Toncheva-Moncheva, Erik Dimitrov, Denitsa Momekova, Petar Petrov, Georgi Grancharov, Stanislav Rangelov
Synthesis of novel polycaprolactone/polyglycidol based block and star copolymers for development of niosomes, **poster**
Erik Dimitrov, Natalia Toncheva-Moncheva, Pavel Bakardzhiev, Rumena Stancheva, Denitsa Momekova, Aleksander Forys, Barbara Trzebicka, Stanislav Rangelov
8. XX National Symposium POLYMERS 2022, Velingrad, Bulgaria, 05–08.07.2022
Preparation of polymer amphiphiles for surface modification of niosomes, **poster, award for best poster**
Erik Dimitrov, Natalia Toncheva-Moncheva, Pavel Bakardzhiev, Rumena Stancheva, Denitsa Momekova, Aleksander Forys, Barbara Trzebicka, Stanislav Rangelov
9. Third Scientific Conference "Innovative Low-Toxic Biologically Active Agents for Precision Medicine BioActiveMed", Kyustendil, 13–15.06.2022
Нови амфифилни съполимери на основата на полиглицидол/поли(ε-капролактон) и полиглицидол/поли(α-цианамил-ε-капролактон) за получаване на високоефективни наноносители на лекарствени вещества, **oral presentation**
Erik Dimitrov, Natalia Toncheva-Moncheva, Pavel Bakardzhiev, Denitsa Momekova, Stanislav Rangelov, Petar Petrov, Georgi Grancharov
10. Scientific Conference INFRAMAT 2022, Hotel Imperial, Plovdiv, 12–14.09.2022
Development of polymer amphiphiles for surface modification of niosomes, **poster**

Erik Dimitrov, Natalia Toncheva-Moncheva, Pavel Bakardzhiev, Rumena Stancheva, Denitsa Momekova, Aleksander Forys, Barbara Trzebicka, Stanislav Rangelov

11. XVIII Poster Session for Young Scientists, PhD Students and Students at UCTM in the Section "Chemical Technologies", UCTM, Sofia, 25.06.2021
    Initiator-free conjugation of oligonucleotides via UV light-induced thiol–ene click reaction for liposomal spherical nucleic acid preparation, poster, award for best poster in the section "Chemical Technologies"
    E. Dimitrov, N. Toncheva-Moncheva, P. Bakardzhiev, K. Mladenova, Jordan Doumanov, Stanislav Rangelov
    Синтез на нови поликапролактон/полиглицидол блокови и звездовидни съполимери за разработване на наноразмерни лекарствени носители – ниозоми, **poster**
    Д. Йорданова, Е. Димитров, Н. Тончева-Мончева, С. Рангелов
12. Third Youth Scientific Conference "Biomedicine and Quality of Life 2021", held online, 02–03.12.2021
    Synthesis and characterization of liposomal spherical nucleic acids via incorporation of nucleolipids synthesized by different approaches, **oral presentation, award for best presentation**
    E. Dimitrov, N. Toncheva-Moncheva, P. Bakardzhiev, K. Mladenova, S. Petrova, P. Videv, V. Moskova-Doumanova, J. A. Doumanov, B. Trzebicka, A. Forys, S. Rangelov
13. XII Scientific Session "Young Scientists in the World of Polymers", Institute of Polymers – BAS, Sofia, 03.06.2021
    Synthesis and characterization of liposomal spherical nucleic acids via incorporation of an original nucleolipid, **poster, award for best poster**
    Erik Dimitrov, Natalia Toncheva-Moncheva, Pavel Bakardzhiev, Kirilka Mladenova, Svetla Petrova, Pavel Videv, Veselina Moskova-Doumanova, Jordan A. Doumanov, Barbara Trzebicka, Aleksander Forys, Stanislav Rangelov
    Development of spherical nucleic acids from novel polystyrene/poly(chloromethylstyrene)/oligonucleotide conjugates via initiator-free click chemistry, **poster**
    Erik Dimitrov, Eleni Vlassi, Natalia Toncheva-Moncheva, Kirilka Mladenova, Jordan A. Doumanov, Stergios Pispas, Stanislav Rangelov
    Novel amphiphilic polyglycidol/poly(ε-caprolactone) and polyglycidol/poly(α-cinnamyl-ε-caprolactone) copolymers as highly effective cannabidiol-loaded nanocarriers, **poster**
    Diana Yordanova, Erik Dimitrov, Natalia Toncheva-Moncheva, Denitsa Momekova, Petar Petrov, Georgi Grancharov, Stanislav Rangelov
14. National Conference INFRAMAT 2021, Pravets, Bulgaria, 08–10.09.2021
    Initiator-free conjugation of oligonucleotides via different click reactions for liposomal spherical nucleic acid preparation, **poster**
    E. Dimitrov, N. Toncheva-Moncheva, P. Bakardzhiev, K. Mladenova, S. Petrova, P. Videv, V. Moskova-Doumanova, J. A. Doumanov, B. Trzebicka, A. Forys, S. Rangelov
    Synthesis of novel polycaprolactone/polyglycidol based block and star copolymers for design of nanosized drug delivery systems – niosomes, **poster**
    Erik Dimitrov, Natalia Toncheva-Moncheva, Pavel Bakardzhiev, Denitsa Momekova, Stanislav Rangelov
15. XI Scientific Session "Young Scientists in the World of Polymers", Institute of Polymers – BAS, Sofia, 10.09.2020
    Нови поликапролактон/полиглицидол блокови и звездовидни съполимери чрез използване на „click" химични реакции: синтез и охарактеризиране, **poster, award for best poster**
    Е. Димитров, Н. Тончева-Мончева, С. Рангелов

Rapid and initiator-free conjugation of oligonucleotides via UV light-induced thiol–ene click reaction, **poster**
P. Denkova, K. Kostova, E. Dimitrov, N. Toncheva-Moncheva, P. Bakardzhiev, S. Rangelov

AWARDS

- Bulgarian Academy of Sciences "Ivan Evstratiev Geshov" Award for the youngest scientists under the age of 30 in the scientific field "Nanosciences, New Materials and Technologies", 2025
- "Prof. Ivan Shopov" Award of the Union of Chemists in Bulgaria for "Outstanding Young Scientist in the Field of Polymers", 2024
- Academician Ivan Yuhnovski Award for "Outstanding Young Scientist in the Field of Organic Chemistry", 2024
- Certificate of Recognition from the President of Bulgaria, Rumen Radev, for "Outstanding achievements in education, contributions to the development of the national science olympiad teams, and enhancing the international prestige of Bulgaria"
- Best Poster Award, International Scientific Conference "Silesian Meetings on Polymer Materials" POLYMAT 2022, Zabrze, Poland
- Best Poster Award, XX National Symposium with International Participation POLYMERS 2022
- Best Poster Award, XI Scientific Session "Young Scientists in the World of Polymers"
- Best Poster Award, XII Scientific Session "Young Scientists in the World of Polymers"
- Best Presentation Award, XIII Scientific Session "Young Scientists in the World of Polymers"
- Best Presentation Award, XV Scientific Session "Young Scientists in the World of Polymers"
- First Prize, XVII Poster Session for Young Scientists, PhD Students and Students at UCTM, section "Chemical Technologies"
- Best Presentation Award, Third Youth Scientific Conference "Biomedicine and Quality of Life 2021"
- Best Poster Award, Annual Scientific Session dedicated to the 155th Anniversary of the Bulgarian Academy of Sciences, Institute of Organic Chemistry with Centre of Phytochemistry
- First and Second Prize for Scientific Supervision of a Student Research Project, Tenth Student Scientific Session of the Bulgarian Academy of Sciences

PARTICIPATION IN SCIENTIFIC PROJECTS

1. **КП-06-ПМ-69/4 (National Science Fund, Bulgaria)** – Development of novel polymer nanocarriers for immobilization and controlled delivery of the proteolytic enzyme serratiopeptidase, 2023–2025
2. **КП-06-НХ43/3 (National Science Fund, Bulgaria)** – Design and characterization of conventional and modified niosomes and hybrid stimulus-responsive in situ gel-forming drug delivery systems based on them for efficient drug delivery, 2020–2023
3. **КП-06-Н23/7 (National Science Fund, Bulgaria)** – Association of bestrophin-1 with membrane domains in model monolayers and epithelial cells – a prerequisite for innovative therapies for retinal degeneration, 2018–2024
4. **ДО1-217/30.11.18 г., BioActiveMed** – Innovative low-toxic biologically active agents for precision medicine (National Scientific Program)
5. **Д01-382/18.12.2020, INFRAMAT** – Distributed infrastructure of centers for production and investigation of new materials and their industrial applications, as well as for conservation, access and e-preservation of artifacts (archaeological and folklore)
6. **КП-06-ПМ59/2 (National Science Fund, Bulgaria)** – Synthesis and investigation of polydopamine nanoantioxidants as a novel therapeutic approach for the treatment of Alzheimer's disease, 2021–2023
7. **ІС-PL/08/2022-2023 (ЕБР)** – Morphological investigation of polymer and polymer-hybrid nanostructures, cooperation between BAS and the Centre of Polymer and Carbon Materials – Polish Academy of Sciences, 2022–2023
8. **№ 17/19.08.2021 г**. – Method for production of polymer particles using MIP technology
9. **ДН 19/8 (National Science Fund, Bulgaria)** – Design of novel supramolecular nanoparticles: spherical nucleic acids with polymeric and liposomal cores
10. **Institutional funding (Bulgarian Academy of Sciences)** – Water-soluble and amphiphilic copolymers and nanoparticles based on them. Controlled polymerization processes
11. **ІС-PL/11/2024-2025 (National Science Fund, Bulgaria)** – Structural characterization of polymer nanosystems using microscopy and radiation-scattering methods
12. **КП-06-Н89/2 (National Science Fund, Bulgaria)** – Cyclic polymer "brushes" – innovative platforms for the synthesis of spherical nucleic acids and delivery of drugs and polynucleotides, 2024–2027

REFERENCES

[1] Dowhan, W. Role of Phospholipids in Cell Function. In *Biological Membranes: Structure, Biogenesis and Dynamics*; Op den Kamp, J. A. F., Ed.; NATO ASI Series H, Vol. 82; Springer: Berlin, Heidelberg, 1994; pp 1–21.

[2] Lingwood, D.; Simons, K. Lipid Rafts as a Membrane-Organizing Principle. *Science* **2010**, *327* (5961), 46–50.

[3] Rangelov, S.; Petrova, E.; Berlinova, I.; Tsvetanov, C. Synthesis and Polymerization of Novel Oxirane Bearing an Aliphatic Double Chain Moiety. *Polymer* **2001**, *42* (10), 4483–4491.

[4] Rangelov, S.; Almgren, M.; Tsvetanov, Ch.; Edwards, K. Synthesis, Characterization, and Aggregation Behavior of Block Copolymers Bearing Blocks of Lipid-Mimetic Aliphatic Double Chain Units. *Macromolecules* **2002**, *35*, 4770–4778.

[5] Rangelov, S.; Almgren, M.; Tsvetanov, Ch.; Edwards, K. Shear-Induced Rearrangement of Self-Assembled PEG-Lipid Structures in Water. *Macromolecules* **2002**, *35*, 7074–7081.

[6] Rangelov, S.; Edwards, K.; Almgren, M.; Karlsson, G. Steric Stabilization of Egg-Phosphatidylcholine Liposomes by Copolymers Bearing Short Blocks of Lipid-Mimetic Units. *Langmuir* **2003**, *19*, 172–181.

[7] Rangelov, S.; Almgren, M.; Edwards, K.; Tsvetanov, C. Formation of Normal and Reverse Bilayer Structures by Self-Assembly of Nonionic Block Copolymers Bearing Lipid-Mimetic Units. *J. Phys. Chem. B* **2004**, *108*, 7542–7552.

[8] Rangelov, S.; Almgren, M. Particulate and Bulk Bicontinuous Cubic Phases Obtained from Mixtures of Glyceryl Monooleate and Copolymers Bearing Blocks of Lipid-Mimetic Anchors in Water. *J. Phys. Chem. B* **2005**, *109*, 3921–3929.

[9] Rangelov, S. Light Scattering and Cryogenic Transmission Electron Microscopy of Vesicles and Other Structures Formed in Water by Mixtures of Copolymers Bearing Lipid-Mimetic Units. *J. Phys. Chem. B* **2006**, *110*, 4256–4262.

[10] Rangelov, S.; Bakardzhiev, I.; Momekova, D.; Ivanova, N.; Marinov, T.; Dimitrov, D. Synthesis and self-assembly of didodecyl ether glycerol-based amphiphilic block copolymers. *J. Macromol. Sci., Part A: Pure Appl. Chem.* **2006**, *43* (9), 861–870.

[11] Momekova, D.; Rangelov, S.; Yanev, S.; Nikolova, E.; Konstantinov, S.; Romberg, B.; Storm, G.; Lambov, N. Long-Circulating, pH-Sensitive Liposomes Sterically Stabilized by Copolymers Bearing Short Blocks of Lipid-Mimetic Units. *Eur. J. Pharm. Sci.* **2007**, *32* (4–5), 308–317.

[12] Momekova, D.; Momekov, G.; Rangelov, S.; Storm, G.; Lambov, N. Physicochemical and biopharmaceutical characterization of dipalmitoyl phosphatidylcholine liposomes sterically stabilized by copolymers bearing short blocks of lipid-mimetic units. *Soft Matter* **2010**, *6*, 591–601.

[13] Bakardzhiev, P.; Rangelov, S.; Trzebicka, B.; Momekova, D.; Lalev, G.; Garamus, V.M. Nanostructures by self-assembly of polyglycidol-derivatized lipids. *RSC Adv.* **2014**, *4*, 37208–37219.

[14] Bakardzhiev, P.; Forys, A.; Trzebicka, B.; Andreeva, T.; Rangelov, S. Unprecedented formation of sterically stabilized phospholipid liposomes of cuboidal morphology. *Nanoscale* **2021**, *13*, 15210–15214.

[15] Momekova, D.; Rangelov, S.; Momekov, G.; Storm, G.; Lambov, N. In vitro biocompatibility study of free and liposome-grafted block copolymers bearing short lipid-mimetic units. *J. Drug Deliv. Sci. Technol.* **2007**, *17* (6), 393–397.

[16] Clayden, J.; Greeves, N.; Warren, S. *Organic Chemistry*, 1st ed.; Oxford University Press: Oxford, UK, 2001

[17] Tokar, R.; Kubisa, P.; Penczek, S.; Dworak, A. Cationic Polymerization of Glycidol: Coexistence of the Activated Monomer and Active Chain End Mechanism. *Macromolecules* **1994**, *27* (2), 320–322.

[18] Toncheva-Moncheva, N.; Bakardzhiev, P.; Rangelov, S.; Trzebicka, B.; Forys, A.; Petrov, P. D. Linear Amphiphilic Polyglycidol/Poly(ε-caprolactone) Block Copolymers Prepared via “Click” Chemistry-Based Concept. *Macromolecules* **2019**, *52* (9), 3435–3447

[19] Mahajan, A. S.; Stegh, A. H. Spherical Nucleic Acids as Precision Therapeutics for the Treatment of Cancer—From Bench to Bedside. Cancers **2022**, 14 (7), 1615.
[20] Barnaby, S. N.; Sita, T. L.; Petrosko, S. H.; Stegh, A. H.; Mirkin, C. A. Therapeutic Applications of Spherical Nucleic Acids. In Nanotechnology-Based Precision Tools for the Detection and Treatment of Cancer; Mirkin, C. A., Meade, T. J., Petrosko, S. H., Stegh, A. H., Eds.; Springer International Publishing: Cham, **2015**; pp 23–50.
[21] Wahane, A.; Waghmode, A.; Kapphahn, A.; Dhuri, K.; Gupta, A.; Bahal, R. Role of Lipid-Based and Polymer-Based Non-Viral Vectors in Nucleic Acid Delivery for Next-Generation Gene Therapy. Molecules **2020**, 25 (12), 2866.
[22] Mendes, B. B.; Conniot, J.; Avital, A.; Yao, D.; Jiang, X.; Zhou, X.; Sharf-Pauker, N.; Xiao, Y.; Adir, O.; Liang, H.; Shi, J.; Schroeder, A.; Conde, J. Nanodelivery of Nucleic Acids. Nat. Rev. Methods Primers **2022**, 2 (1), 24.
[23] Valatabar, N.; Oroojalian, F.; Kazemzadeh, M.; Mokhtarzadeh, A. A.; Safaralizadeh, R.; Sahebkar, A. Recent Advances in Gene Delivery Nanoplatforms Based on Spherical Nucleic Acids. J. Nanobiotechnol. **2024**, 22 (1), 386.
[24] Kapadia, C. H.; Melamed, J. R.; Day, E. S. Spherical Nucleic Acid Nanoparticles: Therapeutic Potential. BioDrugs **2018**, 32 (4), 297–309.
[25] Fairbanks, B. D.; Love, D. M.; Bowman, C. N. *Efficient Polymer-Polymer Conjugation via Thiol-ene Click Reaction.* Macromol. Chem. Phys. **2017**, 218 , 1700073.
[26] Ravanat, J.-L.; Douki, T.; Cadet, J. Direct and Indirect Effects of UV Radiation on DNA and Its Components. J. Photochem. Photobiol. B: Biol. **2001**, *63* (1–3), 88–102.
[27] Lowe, A. B. Thiol-ene "click" reactions and recent applications in polymer and materials synthesis. *Polym. Chem.* **2010**, *1*, 17–36.
[28] Dimitrov, E.; Toncheva-Moncheva, N.; Bakardzhiev, P.; Forys, A.; Doumanov, J.; Mladenova, K.; Petrova, S.; Trzebicka, B.; Rangelov, S. Nucleic Acid-Based Supramolecular Structures: Vesicular Spherical Nucleic Acids from a Non-Phospholipid Nucleolipid. *Nanoscale Adv.* **2022**, *4*, 3793–3803.
[29] Dimitrov, E.; Toncheva-Moncheva, N.; Bakardzhiev, P.; Forys, A.; Doumanov, J.; Mladenova, K.; Petrova, S.; Trzebicka, B.; Rangelov, S. Original Synthesis of a Nucleolipid for Preparation of Vesicular Spherical Nucleic Acids. *Nanomaterials* **2022**, *12*, 3645.
[30] Dimitrov, E.; Toncheva-Moncheva, N.; Doumanov, J. A.; Mladenova, K.; Petrova, S.; Pispas, S.; Rangelov, S. Three-Dimensional Nucleic Acid Nanostructures Based on Self-Assembled Polymer–Oligonucleotide Conjugates of Comblike and Coil-Comb Chain Architectures. *Biomacromolecules* **2023**, *24* (5), 2213–2224.
[31] Gugleva, V.; Ahchiyska, K.; Georgieva, D.; Mihaylova, R.; Konstantinov, S.; Dimitrov, E.; Toncheva-Moncheva, N.; Rangelov, S.; Forys, A.; Trzebicka, B.; Momekova, D. Development, Characterization and Pharmacological Evaluation of Cannabidiol-Loaded Long Circulating Niosomes. *Pharmaceutics* **2023**, *15*, 2414.
[32] Toncheva-Moncheva, N.; Dimitrov, E.; Grancharov, G.; Momekova, D.; Petrov, P.; Rangelov, S.; Forys, A.; Trzebicka, B.; Momekova, D. Cinnamyl-Modified Polyglycidol/Poly(ε-Caprolactone) Block Copolymer Nanocarriers for Enhanced Encapsulation and Prolonged Release of Cannabidiol. *Pharmaceutics* **2023**, *15*, 2128.